International Journal of Heat and Mass Transfer 67 (2013) 469–486

Contents lists available at ScienceDirect

International Journal of Heat and Mass Transfer

journal homepage: www.elsevier.com/locate/ijhmt

Review

An overview of nanoparticle assisted laser therapy

Yildiz Bayazitoglu *, Shiva Kheradmand, Toni K. Tullius

Department of Mechanical Engineering and Materials Science, Rice University, 6100 Main St., Houston, TX 77005, USA

ARTICLE INFO

Article history:
Received 1 July 2013
Received in revised form 6 August 2013
Accepted 7 August 2013
Available online 11 September 2013

Keywords:
Plasmonic
Polymers
Carbon nanotubes
Nanoparticles
Photothermal therapy

ABSTRACT

Interest in minimally invasive and localized treatments for cancer has led toward a dramatic increase in the development of novel nanomaterials as light absorbing agents. The application of nanoparticles as exogenous agents in laser therapy or photothermal therapy (PTT) is rapidly expanding to include nanostructures of various composition and geometries. The particles enhance the magnitude of light absorption resulting in a more precise delivery of energy at lower laser powers and prevent damage to nearby healthy tissue. To date, preclinical and clinical studies of plasmonic photothermal therapy (PPTT) with gold metal nanoparticles have been extensively studied and recently PTT of magnetoplasmonic nanoparticles, carbon nanomaterials, and nano-polymers have shown success in treatment of subcutaneous tumors. In addition, numerical investigations serve as a subsidiary tool for experimental explorations of nanoparticle assisted laser therapy. Since PTT can only be delivered to subcutaneous regions, the introduction of phantom numerical models in nanoparticle assisted laser-induced interstitial thermotherapy (LITT) has shown potential in delivering efficient ablative energy doses to deep-seated tumors. The following review provides experimental and mathematical models that concern metal, inorganic, and polymer nanoparticle assisted laser therapy.

Contents

* Corresponding author. Address: Department of Mechanical Engineering and Materials Science, Houston, TX 77005, USA. Tel.: +1 713 348 6291; fax: +1 713 348 5423.
E-mail address: bayaz@rice.edu (Y. Bayazitoglu).

0017-9310/$ - see front matter © 2013 Elsevier Ltd. All rights reserved.
http://dx.doi.org/10.1016/j.ijheatmasstransfer.2013.08.018

Nomenclature

A_{ij}	interaction matrix
a_n, b_n	Mie coefficients
c_p	specific heat
c	speed of light (Section 3.1.1)
D	diameter
d	distance
E	electric field
E_g	band gap energy
e	electron charge
f	fraction of light scattered
G	particle cross-sectional area
g	anisotropy
H	magnetic field
I	radiant intensity
k	thermal conductivity
k_1	wave vector
k_e	extinction coefficient
L, l	length
M, N	vectors
m	dielectric ratio
m_e	mass of electron
N_T	# of nanoparticles/vol.
n	index of refraction
n_e	density of free electron
P	probability distribution function
P_i	induced dipole moment
P_n	Legendre polynomials
Q_m	metabolic heat generation
Q_R	radiation heat
Q_{abs}	efficiency of absorption
Q_{ext}	efficiency of extinction
Q_{sca}	efficiency of scattering
R, R_1, R_2, R_3	radius
r, p	space/vector
S_c	source term induced by radiation
s	direction
T	temperature
t	thickness
t	time (Section 3)
w	width
x	size parameter

Greek symbols

μ	magnetic permeability
λ	wavelength
ε	dielectric function
ε_p	electric permittivity
ε_0	permittivity in vacuum
ε_B	bulk dielectric
ω	frequency
ω_p	plasma frequency
Φ	scattering phase change
κ	absorption
Θ	scattering angle
ψ, ξ	Bessel function
ψ, η, ξ	directional cosines
θ	polar angle
Γ	damping term
φ	cosine of the angle
α	polarizability
v_F	Fermi velocity
ρ	density

Subscripts

0	incident field
b	blood
c	collimation
d	diffuse
dipole	dipole
Inc.	incident wave
ℓ	indices
local	location of electric field
m	medium
max	maximum
n	vector spherical harmonics
np	nanoparticle
o, e	odd and even
sca	scattered
tissue	biological tissue

Medical

4*T*1	murine breast carcinoma
*B*16/*F*10	murine melanoma
*CT*26	colon carcinoma cell
EGFR	epidermal growth factor receptor
*HER*2	human epithelial receptor 2
*PC*3	human prostate cancer
PEG	polyethylene glycol
SCCVII	squamous cell carcinoma
*SKBR*3	human breast adenocarcinoma
TVT	transmissible venereal tumor
*U*87	human primary glioblastom

1. Introduction

The most common treatments involved for cancers include surgery, radiotherapy, and chemotherapy. In cases where the tumor is not surgically isolatable, radiation and chemotherapy are typically delivered [1]. While proven to be effective in reducing the size of tumors, these treatments also have a high potential to damage healthy cells and may not necrotize the entire tumor. A form of treatment that is both localized and destructive is ideal for cancer therapy. Since early diagnosis and precise treatment are

paramount, nanomedicine holds promise in alleviating the pain, suffering, and death caused by this disease. The small size of nanoparticles, comparable to biomolecules, shows potential to distinguish and interact directly with cell surface receptors of diseased cells. Accumulation of nanoparticles in tumor tissue can further enhance medical imaging and therapeutic modalities. Researchers study the use of nanoparticles in isolated photothermal treatments (PTT) and are in pursuit of determining the most chemically and structurally biocompatible nanoparticle that will provide highly efficient, rapid, and non-invasive means of eliminating localized and widespread tumors, while minimizing adverse effects of surrounding healthy tissue. Conductive metal nanoparticles, such as gold and silver, serve as excellent exogenous materials in laser cancer therapy since the surface electrons induce a unique interaction with the particle nature of light and demonstrate ablative effects by converting light to heat energy. Similarly, carbon based nanostructures and nano-polymers are semi-conducting and can be synthetically engineered with high thermal [2] and electrical [3,4] conductivities that serve as an advantage in enhancing the laser light absorption and subsequent heat conversion involved in PTT.

Laser light sources at different wavelengths entice varying reactions with biological systems, depending on the tissue absorption properties. For example, the near infrared region (NIR), 700–1100 nm, is the region of highest physiological transmissivity and therefore is an optical gateway for laser energy to propagate into the human body with minimal attenuation [5,6]. Light absorbing nanoparticles are optically tunable across the electromagnetic spectrum; therefore, the particles are synthetically tuned to the NIR and the laser is targeted in cancerous area. After incubating absorbing dominated nanoparticles into the cancerous region, the tissues' ability of absorbing radiation photon energy would be greatly strengthened; meanwhile the surrounding healthy tissue still remains to be almost transparent to NIR light. Fig. 1 shows the absorption curves for most common materials that absorb light in the body's tissue: melanin, hemoglobin (Hb), oxyhemoglobin (HbO_2), and water. Notice from Fig. 1 that in the NIR region absorption for these tissues are the lowest.

During the past decade, nanoparticle assisted laser light studies have attracted multidisciplinary research efforts and significantly less laser power is required to achieve the same hyperthermic effects [7]. Investigators are interested in using chemically and structurally biocompatible nanoparticles that will provide highly efficient and minimally invasive means of eliminating tumors. In addition, these nanoparticles also serve as an excellent tool in the field of theranaostics, where these particles simultaneously serve as an optical contrast and therapy agent. There are extensive papers and books that cover specifically the optical properties of different gold geometries [8–14], and reviews that combine optical properties with laser thermal therapy [15–20]. Other manuscripts focus generally on comparing thermal therapy of various nanoparticle geometries [21–25]. There are also reviews that concentrate on gold nanoshells [26,27], gold nanorods (GNR) [28–31], gold nanocages [32], and plasmonic nanoparticles with inner magnetic cores [33–36]. In addition, there have been individual experimental studies that investigate the optical properties of silver nanoparticles [37] and their application in thermal therapy [38,39]. More recently carbon based nanostructures such as nanographene sheets (NGS) [40,41], single-wall carbon nanotubes (SWNTs) [42,43], multi-walled carbon nanotubes (MWNTs) [44], and nano-polymers [45–47] have shown promise in photothermal applications. The purpose of this paper is to provide an overview of the range of optically active nanoparticles along with their biological applications in photothermal therapy and general numerical modeling. In Section 2, there will be a brief description of the optical properties of the metal, inorganic, and polymer nanostructures. The third section will provide a mathematical review describing the various methods on how to calculate the optical properties and then calculate the heat transfer manifested by particle assisted PPT. The last section highlights the progress and results of latest preclinical and clinical studies that demonstrate enhanced PTT with low incident laser power for gold nanoparticles and inorganic materials.

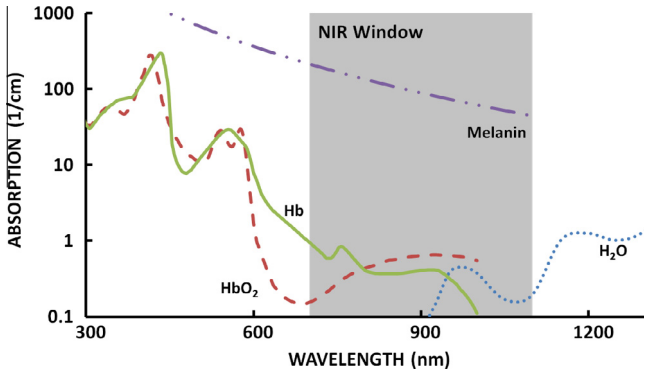

Fig. 1. Absorption spectra in biological tissues adopted (adopted from http://omlc.ogi.edu/spectra/).

2. Optical properties of the nanoparticles

Nanoparticles used in PTT have been synthetically engineered to absorb light in physiological transparent region (NIR) or at a greater magnitude than the biological tissues. To determine whether the nanoparticles are acceptable for biomedical trials, researchers use the extinction, Q_{ext}, absorption, Q_{abs}, and scattering Q_{sca}, efficiencies. The extinction coefficient is the sum of the scattering and absorption efficiencies. The light absorption in the malignant tissue with nanoparticles needs to have a higher absorption coefficient than the surrounding healthy tissue and therefore higher Q_{abs} value than the absorption coefficient of the biological components shown in Fig. 1. When the ratio of absorption to extinction is close to one, absorptive effects surmount the scattering effects and the material is predicted to be favorable in therapeutic modalities. This section describes the optical response in terms of efficiencies for all of the metal and non-metal nanoparticles of different geometries.

2.1. Metal nanoparticles

Metal nanoparticles of solid spheres, shells, rods, and other exotic structures can all be tuned to have peak absorption cross-section in the NIR spectrum with wavelength range $\lambda = 700—1100$ nm. To enhance the efficiency of photothermal therapy, a myriad of different metal nanostructures are engineered into exotic shapes and different sizes. In [48], you can find a gallery of TEM images for (a) 15 nm colloidal gold spheres, (b) 15×50 nm gold nanorods, (c) 160 (core)/17 (shell) nm silica/gold nanoshells, (d) 250 nm Au nanobowls with 55 Au seed inside, (e) silver cubes and gold nanocages, (e) nanostars, (f) bipyramids, and (g) octahedrals just to name a few.

These metallic nanoparticles, such as gold or silver, create uniquely vivid colors resulting from the particle's strong optical resonances called surface plasmon resonance (SPR). When interacting with an electric field, metal structures have a collection of bound mobile electrons on the surface that generate quantized waves, or plasmons, as seen in Fig. 2. The bound electrons oscillate when the frequency of the incident light is in tune with their

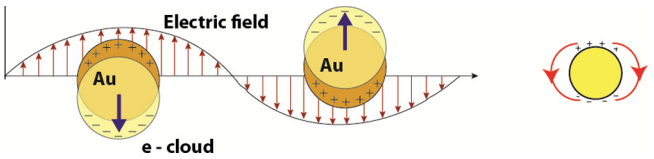

Fig. 2. Plasmonic oscillations induced by an electric field on metallic nanoparticles.

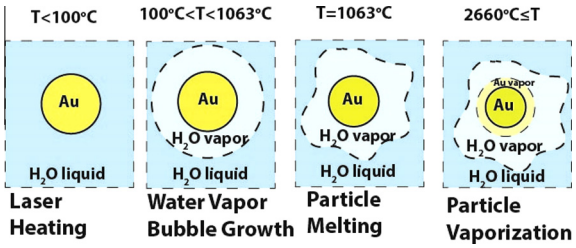

Fig. 3. Generation of plasmonic nanobubble in water.

motion. At this resonant frequency, the surface plasmons are excited from their equilibrium position.

These SPR combined with the size of the metal particles alter the sensitivity and tunability of the optical properties. In addition to changing the size of the particle to tune the optical properties, the particle absorption is extremely sensitive to changes in the medium [49]. Upon interaction with laser light, a high Q_{ext} or Q_{abs} is observed at a narrow breadth that is characterized by a bell shaped curve and a maximum resonant peak value.

Particles with the plasmon-like characteristics have been used in optical and photonic applications and more recently in biomedical applications [10]. Plasmonic metals include Li, Na, Mg, Al, Fe, Cu, Ag, Pt, and Au. Among these, gold is FDA approved, biocompatible, and exhibits good bio-conjugation with biomolecular antibodies and other targeting biomolecules; and is the widely used material in nanoparticles assisted laser therapy [19].

Within the past five years, a new insight has brought more attention to the study of laser heating therapy with nanoparticles. As a laser is induced on a nanoparticle, it begins to absorb the light and as a consequence several environmental thermal processes can occur. First, the surrounding media begins to heat because of the diffuse heating of the nanoparticle [21,50–54]. Next, if the temperature exceeds the saturation temperature, then a vapor or nanobubble may form around the particle [55–60]. If the temperature continues to rise, that may result in the melting of the gold nanoparticle and in turn a gold vapor bubble may be formed around the gold nanoparticle [23,58–62]. This is all portrayed in Fig. 3. More research needs to be conducted to expand the knowledge of the development of nanobubbles.

The solid nanosphere, nanoshell, nanorod, nanocage, nanobelt, nanohexapod, and magnetoplasmonic structures are further discussed. Refer to Fig. 4 for the different geometries and Table 1 for the comparisons of the different resonance peaks between the geometries.

2.1.1. Nanospheres

Nanospheres are solid spherical particles with a high surface area. They can be studied as a single particle or as a collection [63]. Like stated above, when induced by a laser light, the valence electrons of the metal nanoparticles oscillate causing SPR. The SPR peak wavelength is dependent on the shape and size of the metal nanoparticles. When varying the diameter from 20 nm to 60 nm, only a slightly red-shifted wavelength is seen as the diameter increases. The average SPR absorption for nanospheres is around ~525 nm ± 5 [12,15] for gold and slightly lower for silver [37] as shown in Table 1. Recall, the NIR window has wavelengths between 700 nm and 1100 nm. The peak absorption wavelength for nanospheres is not within this range. Because of this, other geometries such as nanoshells and nanorods, which have an easier optical tunability are more favorable for PPTT. Mie theory is generally used to calculate the absorption, extinction, and scattering efficiencies for the spherical shapes. More information on Mie theory will be described in Section 3.1.1.

2.1.2. Nanoshells

Metal nanoshells are different from solid nanospheres because of their geometry. The SPR peak depends highly on the relative size of the dielectric core, shell thickness, and the ratio between the core size to shell thickness. The relative size of the nanoshells can be defined by the aspect ratio given by the ratio of the total radius to core radius, R_1/R_2, as shown in Fig. 4. When varying any of these parameters and also the materials used for the core or the shell, the color of the metal nanoshells can vary across the NIR spectral regions and these nanoshells can also be made to either preferentially absorb or scatter light.

One way to vary the optical properties is to change the material of the core. One of the first dielectric cores used within gold nanoshells is silica, which was introduced by Oldenburg et al. [71]. Silica is non-reactive, chemically inert, and water soluble, making it acceptable for medical applications [27]. Fig. 5 conveys the spectra of the extinction coefficient of gold nanoshells with silica core. Mie theory was used to obtain the results for the figure. This graph proves that metal nanoshells are tunable over a range of wavelengths. When varying the total size of the nanoparticle but keeping the core radius constant, it was observed that the peak SPR shifted. Water was chosen as the exterior medium of the nanoshell because this is a close approximation to the dielectric of the tissue. As the particles become larger, the peak wavelengths shift to the right. Erickson and Tunnell [26] proved that for large particles with small core-to-shell ratios the intensity of the peak will decrease.

Hollow nanoshells (also referred to as hollow nanospheres) are another common nanoshell configuration. When keeping the core constant and varying the shell diameter from 25 nm to 45 nm, the peak absorption shifts from 550 nm to 850 nm, falling in the NIR window [73]. Hollow nanoshells may be more desirable than silica gold nanoshells because researchers are capable of reducing the size of these particles by a factor of four (30 nm in comparison to gold/silica nanoshells which are typically in the range of ~120 nm).

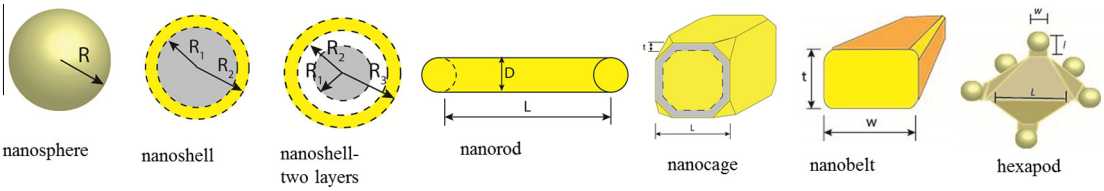

Fig. 4. Various shapes and dimensions for the metal nanoparticles.

Table 1
Optical properties of metal nanoparticles Adapted from [64].

	Dimensions (nm)	λ_{max} (nm)	Q_{abs}	Q_{ext}	Q_{sca}
Nanosphere					
Au [12,14,15]	$R = 20$	521	0.9	0.9	0.0
	$R = 40$	528	2.4	3.0	0.6
	$R = 80$	549	4.0	6.0	2.0
Ag [37]	$R = 76$	466	0.98	1.52	0.52
	$R = 92$	486	1.61	2.1	0.39
Nanoshell					
Au Hollow [3,5,65]	$[R_1, R_2] = [20, 30]$	680	–	9.5	–
	$[R_1, R_2] = [30, 40]$	800	–	13	–
	$[R_1, R_2] = [40, 50]$	980	–	15	–
Si–Au [12,66,67]	$[R_1, R_2] = [60, 170]$	892	3.2	5.2	2.0
	$[R_1, R_2] = [90, 105]$	984	4.2	5.2	1.0
	$[R_1, R_2] = [120, 140]$	1120	3.5	4.1	0.6
(Fe_3O_4/γ-Fe_2O_3)-Si–Au [34–36]	$[R_1, R_2, R_3] = [15.155.200]$	800	1.0	–	–
SPIO-Si–Au [34–36]	$[R_1, R_2] = [-, 90]$	720	0.55	–	–
Nanorod (capped cylinder)					
Au [12]	$[D, L] = [15, 30]$	797	13.5	14.5	1
	$[D, L] = [14.5, 3.3]$	863	15.5	17	1.5
	$[D, L] = [24, 46]$	815	13.5	18	4.5
Nanocage					
Au [68]	$[L, t] = [36.7, 3.3]$	800	11.9	13.5	1.6
Nanobelt					
Au [69]	$[w, t] = [100, 17]$	625	–	–	–
Nano-hexapod					
Au [70]	$[L, w, l] = [60, 13.2, 14.8]$	880	–	–	–
	$[L, w, l] = [33.4, -, 2]$	579	–	–	–

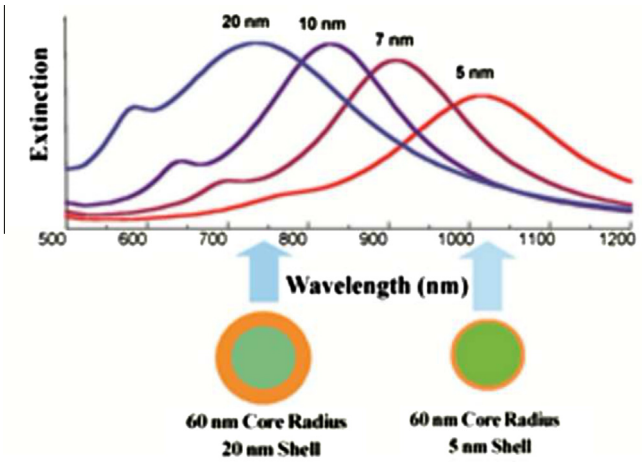

Fig. 5. Extinction coefficient of silica/gold nanoshells in water (from [72]).

These nanoshells are designed to target specific cell types, tissue, tumor, or superficial organs of interest [20]. When comparing the nanoshells to solid nanospheres, because of the variables in the geometry, the nanoshells are easier to tune and the peak SPR can fall in the NIR window.

2.1.3. Nanorods

Jain et al. [12] fabricated gold nanorods in 2006 and are another type of nanoparticle considered for biomedical treatments. This is a cylindrically shaped structure defined by using the aspect ratio. The aspect ratio depends on the ratio of the length of the nanorod to the width of the nanorod, refer to Fig. 4, and the absorption and scattering peaks can be tunable by changing the aspect ratio. The optical properties can be determined computationally using the diffuse dipole approximation (DDA) or the finite difference approximation. More information can be found in Section 3. In [12], they show that the nanorod with the highest absorption peak is the one with the largest aspect ratio and small effective radius. On the other hand, the nanorod with the best scattering has a high aspect ratio with a large effective radius.

GNR have ideal dimensions for interaction with cell surface receptors, are great absorbers, and show characteristic tunability across a range of wavelengths in the NIR region. Using gold nanorods rather than other nanostructures is advantageous because of their smaller size, high absorption coefficient, and narrow spectral bandwidth. However, a possible disadvantage of these nanostructure is their potential to melt and change shape from rod to spherical geometries with high energy [74], prolonged exposure, or use of pulsed lasers [75]. These effects can be minimized but not completely eliminated with polymer or silica coatings [74].

2.1.4. Nanocages

Another nanoparticle that has been fabricated and studied is the nanocage developed by Chen et al. [68]. These structures have a hollow, cube like shape and are more compact than nanoshells. Their porous structure also provides more ability for bio-conjugation and resistance to melting compared to the GNR, refer to Fig 4 [22]. Additionally, the nanocages have absorption at a high NIR band, which contributes to the multipolar SPR band.

Nanocages are typically synthesized based on the galvanic displacement method, a technique where a solid cubical nanostructure with a lower reduction potential (i.e. Ag) is replaced by a metal with a higher reduction potential (i.e. Au) [19,32]. Once this takes place, a redox reaction occurs and silver is oxidized to Ag+. Gold is reduced to the solid form from Au3+ to Au metal. Three silver atoms are exchanged for one gold atom, creating voids in the original cubic structure, and resulting in the subsequent cage-like gold structure [19,32].

2.1.5. Nanobelts

Within the past two years, another geometry that is recently attracting the interest for potential nanoparticle assisted PPT is the nanobelt. A nanobelt is a type of plasmonic nanowire with

sub-100 nm rectangular cross sections, refer to Fig. 5. The gold nanobelt has a small width, comparable to that of a GNR. Anderson et al. [69] revealed that like other gold nanoparticles, the extinction efficiency of the nanobelts were red-shifted upon increase in aspect ratio. For a structure of width of 100 nm and thickness 17 nm, there was a sharp and tunable SPR at 625 nm, near the NIR region. With more tests on tuning this nanoparticle, the nanobelt shows potential for imaging and diagnosis in cancer photothermal therapy. A detailed description for synthesis of nanobelts is described by Wang [76]. The tensile nature of nanobelts may not have the same melting effects observed in GNRs. Studies combining nanobelts and biomedical applications have not been conducted because this is a fairly new geometry.

2.1.6. Nanohexapods

In 2011, Kim et al. [70] developed gold nanohexapods which are a novel class of optically tunable nanoparticles that resemble the structure of a star with branched morphology, see Fig. 4. Nanohexapods consist of an octahedral core and six arm vertices that can be varied in length during synthesis [25,70]. The method for synthesis of the gold hexapods is by seeded growth and more information can be found in [70].

The absorption spectra of the structure typically consists of one peak, unless red-shifted around the NIR region. For the hexapod, there are two peaks, one predominant high intensity peak from the longitudinal SPR of the armed vertices and an additional second peak attributed to the SPR of the central core. The SPR of the nanohexapods shifts from visible (579 nm) to near infrared (880 nm) when increasing the length of the arms. The structure with an arm length of 2 nm and overall length of 33.4 nm had a SPR at 579 nm. When the arm length was increased to 14.8 nm, width of 13.2 nm, and overall length of 60 nm, the SPR was at 880 nm. Branched nanostructures, like nanohexapods, have an increased interest to photothermal conversion because of their sharp tips and high surface to volume ratios [25].

2.1.7. Magnetoplasmonic nanoparticles

Within the past five years, an interest in magnetoplasmonic nanoparticle compounds has been developing. These are nanoshells with a magnetic core (Fe_2O_3, Fe_3O_4) surrounded by a thin layer of plasmonic metal (Ag or Au) [36]. There can also be nanoparticles with a silicon layer sandwiched between the magnetic core and the metal shell [34]. The plasmonic properties of the metal nanoshells in conjunction with the magnetic core properties, which responds to an external magnetic field, holds a potential for guided cancer therapy through a synergistic effect including the use of laser irradiation guided by an magnetic resonance imaging (MRI).

Iron-oxide gold nanoshells have a magnetic core of maghemite (Fe_2O_3) or magnetite (Fe_3O_4) surrounded by a plasmonic gold layer. Larson et al. [36] studied this structure using imaging and other medical applications using particles with an average diameter of ~45 nm and a peak absorption at 540 nm.

Table 2
Optical properties of some nonmetal nanoparticles.

	Dimensions (nm)	λ_{max} (nm)	Q_{abs}
Inorganic			
SWNT [42]	–	1190	0.2
Nano-polymers			
Polypyrrole [77]	[D] = [100]	950	1.0
PEDOT:PSS [45]	[D] = [130]	850	0.5
PCPDTBT [46]	[D] = [289.4]	740	1.0
PCPDTBSe [46]	[D] = [154.3]	–	1.5
EB Polynaniline [78]	[D] = [121.3 ± 24.1]	550	0.8

Iron oxide silica gold (Fe_2O_3–Si–Au) nanoshells are three layered structures that have a magnetic core, a metallic outer shell, and a silicon layer in between the two. The addition of the silica interface between the iron oxide and gold is inserted to allow an easier tuning of plasmonic resonance peaks to the NIR region. Melancon et al. [35] found a high absorbance peak at 650–900 nm for a particle with an average diameter of 90 nm.

2.2. Nonmetal nanoparticles

Nonmental nanoparticles are a rising star in the field of material sciences. These structures include predominately carbon based nanomaterials and nano-polymers. Carbon based nanomaterials and some nano-polymers do not have a characteristic narrow absorption band but can show a high Q_{abs} at a large range of wavelengths. For example, carbon nanotubes have a significantly higher extinction coefficient than biological tissues from 400 to 1000 nm. Table 2 sums up the wavelength and absorption coefficient for some of the nonmetal properties and Fig. 6 provides the different geometries of the non-metal nanoparticles.

2.2.1. Carbon nanomaterials

Carbon based nanomaterials, include NGS [40], SWNTs [42], and MWNTs [44], refer to Fig. 6. Carbon nanomaterials such as NGS and carbon nanotubes (CNTs) are optically active nanostructures with attractive chemical and physical characteristics. The unique properties that make these nanomaterials ideal photothermal agents are mechanical stiffness, photostability, and high thermal and electrical conductivity. Although their electrons are not excited through the plasmon mechanism, they have a strong interaction with light of different wavelengths and a high extinction coefficient.

NGS have an array of carbon bond along a 2D square sheet with size that ranges from 10 nm to 60 nm in lateral length [40] and are gaining tremendous popularity in material sciences. These structure are used in nano-electrical devices such as nanocomposities and semiconductors [79,80] and are currently being tested for biomedical applications [81,82].

To date, CNTs have been widely utilized in electrical systems [2–4,83], and more recently a number of experimental and numerical studies depict how the mechanical stiffness and electronic properties of the CNTs serve as an advantage in not only fields of material science and electronics but also optics and bioengineering [41,42,84–87]. SWNTs are 3D shaped long and thin tubes of sp^2 carbon atoms that resemble a nanographene sheet rolled into a cylinder. The high aspect ratio of the nanostructures, or length to diameter ratio of the nanostructures (i.e. diameter of 4.3 nm and length of 580 nm) result in absorption at a broad range of wavelengths.

Unlike the gold nanoparticles that can be tuned to absorb light in a specified region, it is possible to use different ranges of wavelengths and observe the same effects. In [88], the absorption range

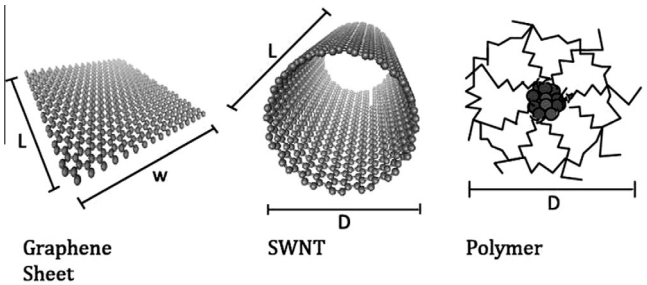

Fig. 6. Various shapes and dimensions for the non-metal nanoparticles.

for SWNTs coincides with tissues in the visible region; however, their extinction coefficient is much higher than the tissue chromophores. There, lasers at a low enough power that would otherwise not induce and optical interaction with the isolated tissue can be applied and have high temperature changes with the presence of SWNTs [43].

2.2.2. Nano-polymers

For polymeric compounds, the electrons are not excited through the plasmon mechanism. To convert a polymer into a semi-conducting material, typically a substance known as a dopant is added to the particle that ionizes the polymer and decreases the interband distance between the valence and conduction. Once this interband distance is reduced, less absorbed energy is required to excite the electrons. The lower the interband distance between the conduction and valence bands are, the easier the transition and excitation of the electrons. Recent discovery of the ability to tune these particles in the NIR region has led the array of different experimental and pre-clinical studies being conducted worldwide by mechanical engineers, medical scientists, and chemists [45–47]. Nano-polymers are now approved for use as drug delivery agents [89,90]; they are being tested for gene delivery [91], PTT [46,92], and as nanocomposites in imaging and thermal treatments [47,93–95].

Polyaniline is a biocompatible organic compound, commonly used to analyze cell division and growth [78]. The polymer is a semiconductor that is electroactive in nature and can be easily manipulated to respond to an incoming electric field. In 2011, this polymer was one of first electrically conductive organic nanoparticles used as exogenous agents for photothermal therapy. While polyaniline derivatives are commonly used for monitoring cell growth and division, the polymer structure based on poly(3,4-ethylenedioxythiophene):poly(4-styrene-sulfonate) (PEDOT:PSS) is a popular compound used in electronics. In addition, PEDOTT: PSS, is not as soluble and biocompatible as the polyaniline and requires an additional polyethlyene glycol coating to increase solubility and decrease possible cytoxicity. Cheng and colleagues [45] performed analysis of this electrically conductive polymer nanoparticle, PEDOT:PSS with a final diameter of approximately 130 nm. This nanoparticle consists of a mixture of two ionomers, repeating units of neutral and ionized copolymers. The particle was tested for toxicity, and was determined to be cytoxic without the presence of a biocompatible coating [45]. With the addition of a branched polyethylene glycol (PEG) coating, the particle was no longer toxic, and cell viability mimicked the control. Advantages of using the polymer nanoparticle PEDOT: PSS-PEG are that they have high photostability over time and high therapeutic efficacy with the use of low laser power (0.5 W/cm^2) [45].

In 2012, another recent non-toxic light-absorbing polymer nanoparticle's optical properties have been studied for potential applications in photothermal cancer therapy by Macneill et al. [46]. In [46], Macneill et al. experimented with a donor–acceptor nanoparticle which had a low band gap properties for photothermal destruction of tumors. The formation of a donor–acceptor bond, also known as the coordination bond, occurs when a pair of electrons from one atom in the highest occupied molecular orbital forms a bond with an atom with an empty electron orbital in the lowest unoccupied molecular orbital. The polymer nanoparticles used for this study were conjugated donor–acceptor compounds 2-ethylhexyl cyclopentadithiophene co-polymerized with 2,1,3-benzothiadiazole (PCPDTBT) or 2,1,3-benzoselenadiazole (PCPDTBSe). These nanoparticles are non-toxic until irradiated by NIR light. The characteristic of this bond type is of interest because of the position of the valence band in relation to the conduction band. In particular one can control the size of the band gap, and hence increase the conductivity with decrease in band gap size [46]. It was hypothesized that the lower the band gap energy, E_g, the greater the absorption coefficient. However, in this study, the chemical nature of elemental sulfur caused a slightly greater energy band gap yet stronger absorption. The polymer with PCPDTBT has an E_g = 1.46 and a much higher absorption coefficient compared to the nanoparticle PCPDTBSe with a band gap value of E_g = 1.36. The stronger absorption by sulfur in comparison to selenium is also confirmed by a study conducted by Gibson et al. [96], where a single atom was varied and the conjugated molecule with sulfur had the highest absorption coefficient. Chen et al. [77] used the polymer polypyrrole for in vivo PPT studies.

Fig. 7 shows the absorption peaks of the different polymer nanoparticles tuned to the NIR region.

3. Mathematical model

As shown in the previous section, there has been a variety of nanoparticles with different shapes, sizes, and composition proposed that may be used for tumor/cancer diagnosis and treatment. Although experimental investigation would be the primary tool to explore the medical applications of nanoparticles, it is better to investigate numerically by creating an approximated model and simulating the effects of the nanoparticles exposed to a laser. This could be useful in accelerating the research by reducing research costs and the un-necessary repetition of work and efforts. Several projects have been carried out with a goal to develop accurate numerical investigations for experimental explorations of nanoparticles in medical applications toward tumor cancer diagnosis and treatment [98–100]. This section provides an overview of methods on solving for the optical properties and also the typical mathematical formulations when modeling nanoparticle based treatment like plasmonic photothermal therapy (PPTT) and laser-induced interstitial thermotherapy (LITT).

3.1. Finding the optical properties

Before we can model nanoparticle laser treatments, knowledge of the optical properties are necessary. There are various methods proposed to numerically calculate the properties for various geometries like Mie theory [9,13,98,101–103], discrete dipole approximation (DDA) [13,18,101,104–106], boundary element method (BEM) [13,107], finite element method (FEM) [101], and finite difference time domain method (FDTD) [101,108,109] to name a few. These methods were used to produce the absorption and extinc-

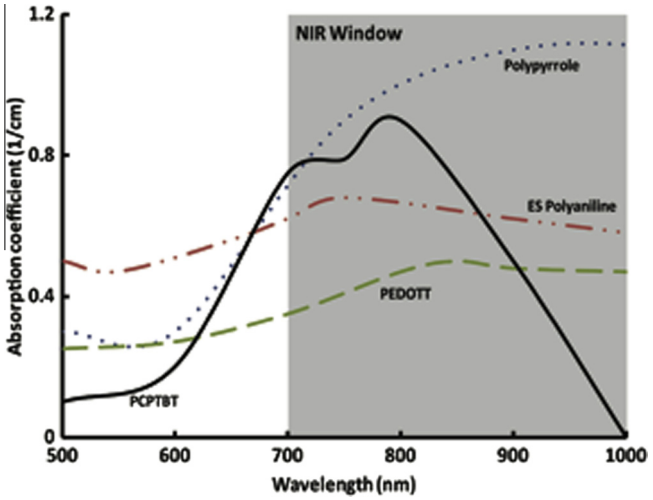

Fig. 7. Absorption coefficient for nano-polymers (adopted from [45,46,77,97]).

tion coefficient graphs for various geometries. For this section, only Mie theory and DDA will be described briefly.

3.1.1. Mie theory

Mie theory was first introduced by Gustav Mie in 1908 [103]. This is an analytical solution of Maxwell's equations describing the scattering of an incident plane wave by a spherical, isotropic, and non-magnetic particle in a non-absorbing medium. Detailed descriptions of this method can be found by van de Hulst [8] and Bohren and Huffman [9] and briefly given here. Assuming no sources, Maxwell's equations are

$$\begin{aligned}\nabla \times H(r,t) &= \varepsilon_p(r)\frac{\partial E(r,t)}{\partial t},\\ \nabla \times E(r,t) &= -\mu(r)\frac{\partial H(r,t)}{\partial t},\\ \nabla \cdot E(r,t) &= 0,\\ \nabla \cdot H(r,t) &= 0,\end{aligned} \tag{1}$$

where H is the magnetic field, E is the electric field, ε_p is the electric permittivity, and μ is the magnetic permeability. Manipulating the equations using Fourier transform, the time varying electromagnetic field in an isotropic medium must satisfy the Helmholtz equations written as

$$\begin{aligned}\nabla^2 E + k_1^2 E &= 0,\\ \nabla^2 H + k_1^2 H &= 0,\end{aligned}$$

where $k_1^2(r) = \omega(r)\varepsilon_p(r)\mu(r)/c^2$ is the wave vector. The parameter ω is the frequency and c is the speed of light. Spherical harmonics can be used to solve the Helmholtz equations. In this approach, E and H are replaced by vectors M_n and N_n. The subscript, n, represents the different vector spherical harmonics used to describe the polar contributions to the scattered field, i.e. $n = 1$ dipolar, $n = 2$ quadripolar, etc. The scattered fields are related to vector spherical harmonics through the series,

$$\begin{aligned}E_{sca} &= \sum_{n=1}^{\infty} E_n(ia_n N_{e\ell n} - b_n M_{o\ell n}),\\ H_{sca} &= \sum_{n=1}^{\infty} E_n(ib_n N_{o\ell n} - a_n M_{e\ell n}),\end{aligned}$$

where $E_n = i^n E_0 \frac{2n+1}{n(n+1)}$ and E_0 is the incident field. The subscripts 0 and e are the odd and even branches of the azimuthal solution to the vector form of the Helmholtz equation and ℓ denotes the terms of the Legendre and Bessel polynomials. The parameters a_n and b_n are the Mie coefficients which determine the amplitudes of the vector spherical harmonics when excited with a particular wavelength of light. These values are given by

$$\begin{aligned}a_n &= \frac{m\psi_n(mx)\psi_n'(x) - \psi_n(x)\psi_n'(mx)}{m\psi_n(mx)\xi_n'(x) - \xi_n(x)\psi_n'(mx)},\\ b_n &= \frac{\psi_n(mx)\psi_n'(x) - m\psi_n(x)\psi_n'(mx)}{\psi_n(mx)\xi_n'(x) - m\xi_n(x)\psi_n'(mx)},\end{aligned} \tag{2}$$

Here, ψ_n and ξ_n are the Bessel functions, x is the size parameter defined by $x = 2\pi n_m R/\lambda$, and m is the ratio between the dielectric functions between the spherical nanoparticle and the surrounding medium, $m = \varepsilon/\varepsilon_m$. The dielectric function for the nanoparticles is generally described using the Drude-Lorentz model [9,110]

$$\varepsilon = \varepsilon_B - \frac{\omega_p^2}{\omega^2 + \Gamma^2} + i\frac{\omega_p^2\Gamma}{\omega(\omega^2+\Gamma^2)}, \tag{3}$$

where ε_B is the bulk dielectric of the material, $\Gamma = \Gamma_0 + \frac{v_F}{R}$ is the damping term, and $\omega_p = \sqrt{\frac{4\pi n_e e^2}{\varepsilon_0 m_e}}$ is the plasma frequency of the free electron gas. The plasma frequency is dependent on the particular metal where m_e is the mass of an electron, n_e is the density of the free electrons for the metal, e is the electron charge, and ε_0 is the vacuum permittivity. The damping term is dependent on the radius of the particle, R, and the Fermi velocity, v_F.

When evaluating the electromagnetic scattering response, the extinction, absorption, and scattering efficiencies are used. Using the Mie scattering coefficients, the efficiencies can be described by

$$\begin{aligned}Q_{ext} &= \frac{2}{x^2}\sum_{n=1}^{\infty}(2n+1)\mathrm{Re}(a_n + b_n),\\ Q_{sca} &= \frac{2}{x^2}\sum_{n=1}^{\infty}(2n+1)(a_n^2 + b_n^2),\\ Q_{abs} &= Q_{ext} - Q_{sca}.\end{aligned} \tag{4}$$

A Fortran routine called ABSCAT can assist in solving the absorption and scattering coefficients [111] and MATLAB programs have been described and documented in [102]. This method is only for spherical geometries.

3.1.2. Discrete dipole approximation

Purcell and Pennypacker [105] in 1973 pioneered the discrete dipole approximation in approximating the extinction, absorption, and scattering cross sections for dielectric grains of arbitrary shapes. For this method, each particle is modeled as an assembly of a finite number of elements. These elements are considered to be sufficiently small such that only dipole interactions with the incident electric field and induced fields in neighboring elements need to be considered. According to Draine and Flatau [106], the solution of the Maxwell's equations reduce to an algebraic problem of many coupled dipoles. Each dipole requires the knowledge of the dipole moments of the external electric field and the electric fields of the neighboring dipoles. The expression to describe the electric field of one dipole is [101]

$$E_{dipole} = \frac{e^{-\frac{i\omega d}{c}}}{4\pi\varepsilon_0}\left[\frac{\omega^2}{c^2 d}\hat{r}\times p\times\hat{r} + \left(\frac{1}{d^3} - \frac{i\omega}{cd^2}\right)[3(\hat{r}\cdot p)\hat{r} - p]\right],$$

where d is the distance to the sampling point, $\hat{r}$ is a unit vector associated with a vector r which is taken from the dipole to the location at which the electric field is sampled, and p is the vector associated with the induced dipole moment. Each dipole has an induced dipole moment,

$$P_i = \alpha_i E_{local},$$

where α_i is the polarizability of the material associated with the each dipole moment and E_{local} is the electric field at r_i due to the incident wave, $E_{inc,i}$, and the contributions of the electric fields from all the other dipoles, E_j as shown by

$$E_{local} = E_{Inc.,i} + \sum_{\substack{j=1\\ i\neq j}} E_j = E_{Inc.,i} + \sum_{\substack{j=1\\ i\neq j}} A_{ij}P_j,$$

where A_{ij} is the interaction matrix between all the dipoles describing the particle. Once the scattered electric field is determined, then the scattering efficiency may be calculated by

$$Q_{sca} = \frac{k}{\pi r^2 |E_i|^2}\int_{dS} |E_{sca}(r')\cdot\hat{r}|^2 dS.$$

Fast Fourier Transform and complex conjugate gradient are few methods that can be used to perform efficient methods to solve the linear system. DDSCAT is an open source Fortran based code created by Draine and Flatau [112] which uses the DDA to compute the optical response of both metallic and dielectric nanostructures.

3.2. Nanoparticle assisted laser modeling

In a clinical setting of nanoparticle laser therapy, the nanoparticles are delivered to the target sites by either direct injection or by capsulated drugs and intravenously via blood circulation [113]. If the nanoparticles are in the blood stream, eventually they are deposited into the cancerous region due to vasculature abnormalities in the tumorous tissue. Researchers worldwide are striving for effective ways to conquer cancer by collaborating with multidisciplinary areas. Some scientists concentrate on modeling laser propagation and laser energy distribution, while others investigate the bioheat process to provide supplemental hyperthermia information. Few studies model the physics of the entire process. This next section describes the computational model representing the process of laser heating of nanoparticles in the body.

3.2.1. PPTT computational methods

Because particle assisted laser therapy has a real potential in medicine, accurate mathematical modeling predicating the temperature distribution is important for in vivo trials and clinical usage. Once the nanoparticles are inserted into the body and a laser is heating the area, the optical properties of the tissue around the nanoparticles are affected causing a change in the thermal response. The Radiative Heat Transfer (RTE) equation is the most common method used to represent the light propagating in biological tissue given by

$$\frac{\partial I(r,s,t)}{c\partial t}+\frac{\partial I(r,s,t)}{\partial s}=-k_e I(r,s,t)+\frac{\sigma}{4\pi}\int \Phi(s,s')I(r,s',t)d\omega' + S_c(r,s), \tag{5}$$

where $I(r,s,t)$ (W/m^2/sr) is the radiant intensity related to fluence. The parameters r and s represents the space and direction coordinates, respectively. The term, $k_e = \kappa + \sigma$, where κ (1/m) and σ (1/m) are the local absorption and scattering coefficients. The parameter, $\Phi(s,s')$ (1/sr), is the scattering phase function which describes the scattering contribution from the direction s to s'. Various expressions can be used to calculate this scattering phase function including Chu and Churchill's expression [114,115] and the Henyey–Greenstein (HG) function [116]. Generally, the HG probability density function is used to calculate the deflection scattering [116] and has been shown to adequately describe the angular distribution of scattered light for most macroscopic tissue. The HG function is expressed by

$$\Phi_{HG}(s,s')=\frac{1}{4\pi}\frac{1-g^2}{[1+g^2-2g(s\cdot s')]^{3/2}} =\sum_{n=0}^{N}\frac{2n+1}{4\pi}g^n P_n(\cos\Theta), \tag{6}$$

where P_n are the Legendre polynomials of order n. The scattering angle and the anisotropy are calculated as

$$\Theta = s_i\cdot s_j' = \xi_i\xi_j+\eta_i\eta_j+\mu_i\mu_j,\quad g=\int_0^{4\pi}P(s\cdot s')s'd\omega,$$

respectively, where

$$\mu=\sin\theta\cos\psi,\quad \eta=\sin\theta\sin\psi,\quad \xi=\cos\theta$$

are the directional cosines represented using the polar angle θ and azimuthal angle ψ and P is a probability distribution function. The term, g, indicates the isotropic scattering and varies from -1 to 1 and 0: 1 is for forward scattering and -1 is for backward scattering. Dombrovsky et al. [99,117,118] uses a transport approximation for the phase function where Φ is the sum of the isotropic component and a term describing the peak forward scattering,

$$\Phi(\varphi_{sca})=(1-\varphi_\lambda)+2\varphi_\lambda\delta(1-\varphi_{sca}).$$

Here, $\varphi = \cos\theta$ is the cosine of the angle for scattering, *sca*, or wavelength, λ. From Eq. (5), $S_c(r,s)$ represents source term induced by the irradiation and is defined by

$$S_c=\frac{\sigma(r)}{4\pi}\int_0^{4\pi}\Phi_{HG}(s,s')I_c(r,s')d\omega'.$$

The intensity of radiation, $I(r,s,t)$, is composed of two terms: a collimation irradiance, $I_c(r,s,t)$, and a diffusion radiant intensity, $I_d(r,s,t)$, such that

$$I(r,s,t)=I_c(r,s,t)+Id(r,s,t).$$

The RTE equation, Eq. (5), defines the change in intensity as the sum of the loss due to absorption and scattering (first term on RHS) with the gain due to scattering and the energy source (second and third term on the RHS). The continuous waved (CW) laser, with a power range 1–5 W, is commonly used in PPTT to treat the tumors; therefore, the temporal term in Eq. (5) is considered negligible. This equation is an integral–differential expression and is difficult to directly solve. Approximate answers can be found using optical diffusion approximation [118,119], P1 approximation [120–122], and delta P1 approximation [117,119,123–125].

The delta P1 approximation splits the phase function into a forward directed (unscattered) component and diffusely scattered component [123,124,126] which is approximated by the phase function,

$$\Phi_{\delta-P1}=[2f\delta(1-s\cdot s')]+(1-f)[1+3g(s\cdot s')]. \tag{7}$$

The parameter, f, defines the fraction of light scattered directly forward and g represents the asymmetry scattering. The second term in Eq. (7) describes the diffuse scattering, which is a scaled version of the approximated phase function for the standard P1 approximation [123]. The first term, which includes a δ function, corresponds to the scattering in the forward direction. Substituting Eq. (7) into Eq. (5) becomes

$$\frac{\partial I}{\partial s}=-k_e I+\sigma f I+\frac{(1-f)\sigma}{2\pi}\int[1+3g(s\cdot s')]Id\omega'+S_c.$$

The variables f and g are found requiring the first two moments of the delta P1 phase function, $g_1 = f + (1-f)g$ and $g_2 = f$, to correspond to the first two moments of the HG phase function, Eq. (6), which are given by $g_n = g_1^n$ [123]. This yields to

$$f=g_1^2,\quad g=g_1/(g_1+1). \tag{8}$$

You then proceed to solve the RTE. The delta P1 approximations scale the optical properties. The P1 approximation and delta P1 approximation are computationally efficient; however, the accuracy of the method is compromised for non-plane parallel and multi-dimensional computations [120,121].

Another computational method used to examine the photon transport in biological tissue is the statistical based Monte Carlo ray tracing method that is mathematically equivalent to solving the RTE equation [126–128]. This computational method simulates a "random walk" of photons in a scattering and absorbing medium. The Monte Carlo method is useful for solving complex geometries and easy to implement; however, in order to be accurate, it requires a number of photons that are traced and therefore computationally expensive [23]. An open source code written in C, called Monte Carlo Modeling of Light Transport in Multi-Layered Tissues (MCML) is used to help simulate some calculations [126]. Lin et al. [129] tried to detect cancerous cells with nanoparticles using the Monte Carlo method. Feng et al. [130,131] used supercomputers to predict real time fluence control using supercomputers. In [132], the Monte Carlo method was used in the study of burning efficiency of different nanoshells with different thick-

nesses and substances inside the shell. The result was that the hollow nanospheres exhibit the best efficiency.

The RTE equation and the Monte Carlo method describe the light transport in the macroscale. To adjust for the optical changes discussed in Section 2, caused by laser light passing through the body heating the nanoparticles, expressions for the absorption and scattering by both the tissue and the nanoparticles are developed. Generally, an idealized condition of uniformly distributed nanoparticles, as depicted by Fig. 8 for a liver tumor, is enforced [98,119,121,133]. Therefore, the overall absorption, κ, and scattering, σ, are defined by the linear relationship between the tissue and the nanoparticles [119–121,129,130,134,135] expressed by:

$$\kappa = \kappa_{np} + \kappa_{tissue}, \quad \sigma = \sigma_{np} + \sigma_{tissue},$$

where *np* and *tissue* indicate the properties for the nanoparticles and biological tissue, respectively. The parameters, κ_{np} and σ_{np}, are functions of the absorption, Q_{abs}, and scattering, Q_{sca}, efficiency such that [119–121,129,130,134,135].

$$\kappa_{np} = GQ_{abs}N_T, \quad \sigma_{np} = GQ_{sca}N_T,$$

where N_T is the number of nanoparticles per unit volume and G is the particle cross sectional area projected onto the plane perpendicular to the incident beam. For nanospheres and nanoshells, $G = \pi R^2$. The parameters Q_{abs} and Q_{sca} are calculated using the methods described in Section 3.1.

Under a normal circumstances, the nanoparticles inside the biological tissues or cells are non-uniformly distributed [136–139] and more computational studies are still necessary to describe this.

Modeling the human body can be very complicated because of the many mammalian physiological actions such as perspiration. In 1948, Pennes presented the bio-heat transfer equation [140–142]. Since then, many people have modified this expression to account for more sophisticated phenomena to include convection, metabolism, and evaporation in addition to conduction and perfusion. The bio-heat transfer equation is given by

$$\rho c_p \frac{\partial T}{\partial t} = -\nabla(k\nabla T) + c_b\omega_b\rho_b(T_b - T) + Q_m + Q_R, \tag{9}$$

where the density, specific heat, and thermal conductivity of the tissue are denoted by ρ (kg/m^3), c_p (J/kg °C), and k (W/m °C), respectively. Similarly, T_b (°C), c_b (J/kg °C), ρ_b (kg/m^3), and ω_b (kg/m^3 s) are the temperature, specific heat, and density of the blood and the blood perfusion rate, respectively. Blood perfusion rate can be defined as the rate at which nutritive-rich (and possible medicated) arterial blood reaches capillaries in the tissue. The metabolic heat generation, Q_m, is the heat caused by the chemical reactions taking place within the tissue and the external heat caused by the laser is denoted by Q_R, which is solved using the RTE equation or the Monte Carlo method. The first term on the LHS of Eq. (8), $\nabla(k\nabla T)$, describes the heat transfer in the body in the body caused by conduction, and the convection term is by $c_b\omega_b\rho_b(T_b - T)$. With the boundary conditions in place, the bio-heat equation models the temperature of the tumor and its surrounding healthy tissue.

Gold nanoshell-assisted PPTT was numerically investigated by concentrating on the mechanical aspects of the problem, namely radiative transport, distributed heating, and thermal conduction [120,121,143]. These work provide a 1D thermal model utilizing the P1 approximation to simulate the penetration of laser radiation and subsequent heating of 1 cm slabs of nanoshell embedded tissue exposed to a 633 nm collimated light source. The sensitivity of nanoshell density, laser power, and laser arrangement on thermal profiles are analyzed. Vera and Bayazitoglu [121] showed that adding too many nanoshells or by having the power source too high can cause overheating in the entry region and the rear region heated only by conduction. This results in an undesirable temperature differential. To avoid this issue, a dual laser approach was proposed and the effect of a two-beam case without varying laser power is presented. Without inserting invasive laser applicators into the tissues, a conformal mode of hyperthermia could be achieved with a much lower laser power compared to the conventional PPT and LITT without nanoparticles. In [121], results show that the required parameters of hyperthermia will be satisfied by not inserting the gold nanoparticles into the body. Xu et al. [133] investigated the feasibility of nanoshell assisted laser treatment by simulating other organ tumors other than subcutaneous tumors, particularly tumors growing in the clearance organ liver. It

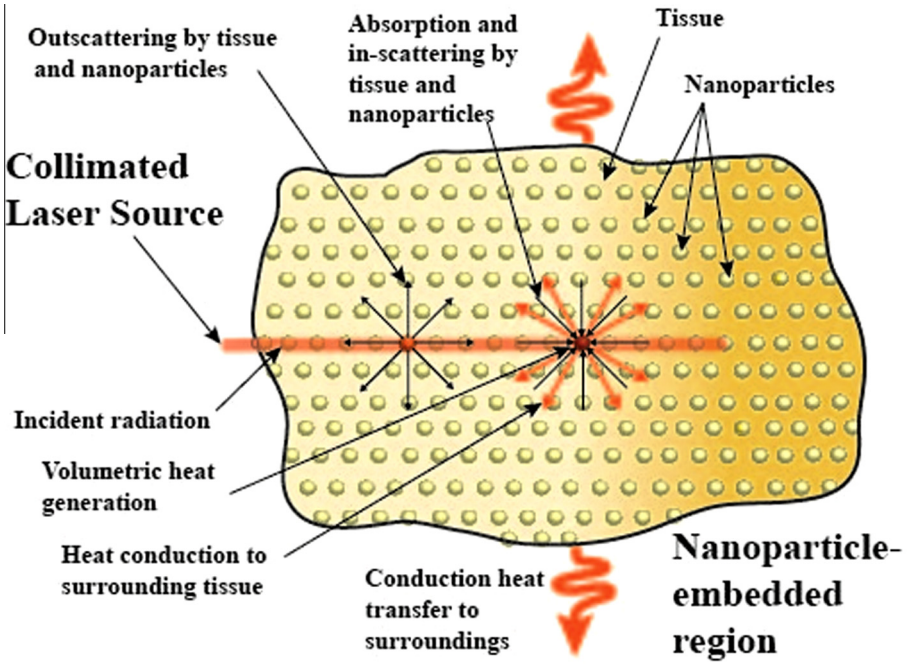

Fig. 8. Schematic of nanoparticle assisted photothermal therapy.

was found that with a nanoshell retention ratio of 8/1 or higher, about half of the liver tumor was ablated; however, some of the surrounding healthy liver tissue was destroyed as well.

3.2.2. LITT computational methods

Another minimally invasive treatment for cancer/tumors is LITT [144–146]. The most commonly used sources for LITT are Nd: YAG laser (1064 nm) or diode lasers (800–980 nm), where approximately 3–10 watts is applied for 10–20 min [146]. For LITT, laser applicators such as fibers or diffusing applicators are surgically inserted into the malignant tumor as shown in Fig. 9. For LITT, a flexible glass fiber transmits laser light into the tumor area. Heat is generated by the absorption of energy radiated by a flexible glass fiber. This heat is then transferred by means of conduction to the neighboring cells. The extent to which it is transmitted is dependent on the energy applied by the laser and the duration of application, perfusion cooling by blood, and the properties of the tumor. Bigger sized tumor could possibly be burnt out to the point of necrosis (cell death).

Depending on the type of tissue the tumor is in, the tumor's thermal and optical properties can vary. Applying the correct level of energy specified for the specific tissue for the right about of time can result in the desired necrosis. Though the temperature at which this occurs varies by cancer type and the values for liver cancer are well established. For example, enzymes in the tumor cells for a liver are permanently damaged, causing necrosis, when the temperature range is 42–45 °C [147]. In the same cancerous cells, when the temperature is between 60–140 °C, the cells will die almost immediately and between 100–300 °C, water in the cell vaporizes, affecting adjacent cells. When the temperature is greater than 300 °C, carbonization occurs and the cell is totally burnt.

Reaching temperatures too high are extremely undesirable because overheating can result in carbonization of cells. If the cells are burnt to carbon, the absorption level of the cells may alter and the laser light may not be able to penetrate the tissue. Also, the thermal properties of the human tissue are dependent of the water content within in them. Therefore, a water loss will change the way the cells react over time even if the laser is applied in a constant manner. Because of the reasons stated above, current developments in LITT are dedicated to developing accurate real time imaging techniques. The use of ultrasound or even MRIs while performing LITT can give doctors real-time feedback as to the progress of the treatment and thermal distribution in cells. When inserting photonic nanoparticles, sharp changes in temperatures at the interface of the tumor and healthy cells can occur. This implies that doctors can avoid undershooting and overshooting the temperature target, which would either leave tumor cells still in the body or cause damage to adjacent healthy cells.

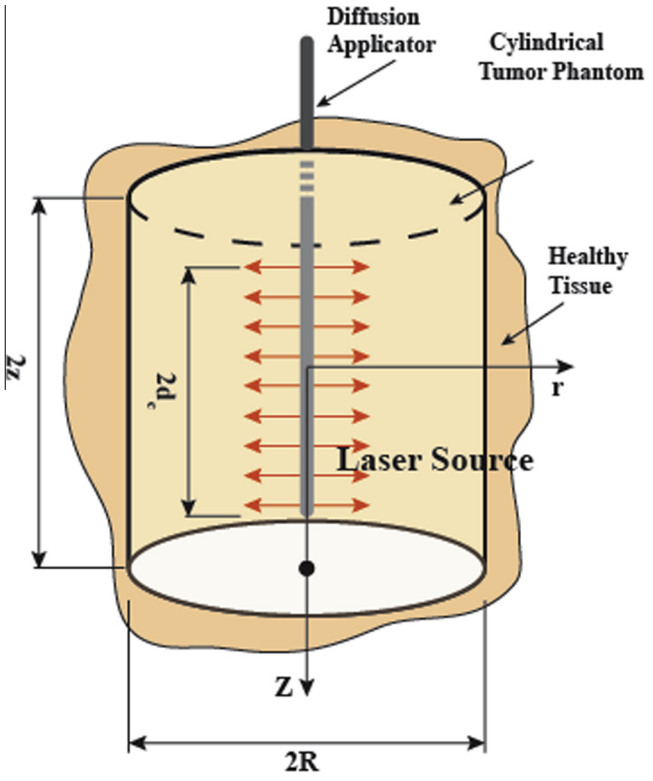

Fig. 9. Schematic of LITT based treatment.

LITT has been used for a variety of cancers from brain to breast cancer; however, different types of biological tissues have distinct absorption properties and may require different treatments. Therefore, simulating a 3D thermal model of LITT to accurately predict the spatial distribution of laser fluence rate, laser energy absorption, and subsequent thermal response of tissue is very important, especially concerns of cell survival due to high temperatures of fatal organs. The current method of choice for this process is using the computationally intensive and expensive inverse 3D Monte Carlo method [126–128,148–150]. Another method to simulate LITT includes the not so accurate but computationally efficient diffusion approximation of the RTE equation [119–121,125,151–153] which approximates the spatial distributions of laser fluency rate and absorption during the treatment.

LITT assisted with nanoshells to enhance the heating effect have been studied experimentally and numerically using phantoms [125,131,154]. In 2009, Fuentes et al. [125] experimented with gold-coated, silica-core nanoshells with core diameters of 110 nm and 180 nm. For these experiments, 1.5 wt% agar gel cylindrical phantoms were used and divided into two layers: the lower layer contained the nanoshells while the upper layer was agar gel only. The dimensions of the cylindrical phantom were 23 mm wide by 69 mm high. All experiments were performed in a clinical 1.5 T MRI scanner and the 2D temperature images were taken in the vertical plane running down through the center of the phantom. The laser wavelength was tuned to 808 nm for these experiments and the output power was varied from 0.32 to 1.2 W. The delta P1 approximation was used to calculate the power density. Temperature distribution is obtained by using commercial finite element modeling (FEM) software (COMSOL MULTIPHYSICS®, Comsol Inc., Burlington, MA).

Another computational study was given by Xu et al. [98] which focused on understanding the therapeutic effects of treatment conditions including laser wavelength, power, exposure time, concentrations of tailored nanoparticles, and optical/thermal properties of the tissue under nanoparticle assisted LITT. This study found that when using absorbing preferential nanoparticles as the photothermal agent, the fluence rate distributions will weaken in terms of lowering fluence rate peaks and reducing laser penetration depth. However, the local enhancement in absorption induced by nanoparticles is so significant that the reduced fluence rate will be balanced out and the eventual medical hyperthermia is greatly enhanced by using nanoparticles. In addition, the results indicated that with constant laser illumination, an increase in nanoparticle concentration beyond a certain range has an insignificant impact on hyperthermia.

Researchers strongly believe that PPTT or LITT treatments can be most effectively approached by the marriage of the advanced methods for simulating radiative transport and bio-heat transport with some (possibly MRI-guided) temperature imaging for validation of predictions. To fully understand the potential of nanoparticle assisted laser therapy, as well as to develop treatment/planning

algorithms to maximize efficacy, advanced models need to be further developed and validated. These models and software need to be effective and easy to use by clinical doctors. Also, these models are at the macroscopic scale, and may be useful in determining first estimates of the efficacy of nanoparticle heating as bulk properties of nanoparticles and matrix medium are used to determine the overall effects of the combined system. However, these models may introduce errors since this phenomenon is at the nanoscale. More studies between the nanoparticle and the water heat transfer interface at the nanoscale need to be conducted. More accurate and comprehensive modeling of the interactions between cancerous tissue, laser irradiation, and nanoparticles for the PPTT and LITT are needed.

4. Laser therapy with nanoparticles

As shown in Section 2, having the nanoparticles injected into the tissue enhances the optical properties and destroys the cancerous tissue. There have been a few in vivo and in vitro studies that include nanoparticle assisted PPT. Table 3 summarizes a few studies by providing the type of nanoparticle, laser used, etc. This section gives a few in vivo and in vitro investigations that have been conducted while using metal and non-metal nanoparticles. It also gives some examples of using nanoparticles as drug delivery vessels.

4.1. Laser therapy with metal nanoparticles

When compared to nanospheres, nanoshells are more favorable for in vivo therapy and imaging applications because the SPR peaks are within the NIR window. In 2003, Hirsch et al. [157] conducted the first demonstration of an in vivo treatment of silica/gold nanoshells for the treatment of carcinoma tumors in mice. Tests on nanoshell density, light intensity, and duration of illumination were monitored using MRI thermal

imaging and it was found that fluctuations in temperature sufficient enough to induce irreversible tissue damage were 6.6 °C after 4–6 min of irradiation while nanoshell-free control samples showed a temperature increase of 4.7 °C. This was an increase that is considered to be safe for cell viability. Also, the highest change in temperature was found at a depth of 2.50 mm.

The first in vitro study to couple bioimaging and cancer therapy applications using nanoshells was in 2005 by Loo et al. [162]. This study targeted against human epithelial receptor 2 (HER2) to treat breast cancer cells and confirmed that the extent of absorption and scattering depend upon the overall size of the nanoshell, while the surface plasmon resonance depends upon the core/shell ratio. In [162], the therapeutic nanoshell, with a 100 nm core and 4 nm shell, had a maximum absorption, while the nanoparticle with optimal scattering characteristics had a 200 nm core and 11 nm shell. When imaging was completed, greater silver staining intensity was seen in cells exposed to anti-HER2 nanoshells compared to controls, and the cell samples were immediately irradiated by 820 nm NIR laser light for 7 min. The laser power was controlled at 8 mW/cm^2. Cell death was observed only in cells treated with anti-HER2 nanoshells and was not observed in cells treated with either nanoshells conjugated to a nonspecific antibody or NIR light alone. Although animal models have demonstrated success, clinical trials on humans have yet to be conducted as the carcinogenicity of the silica nanoshell core remains questionable. It would be more desirable to have nanoshells that are made purely of gold such as hollow nanoshells.

Lu et al. [156] conducted an in vivo study involving hollow nanoshells with a mean diameter of 43.5 ± 2.3 nm and a mean shell thickness of 3–4 nm. Four hours after injecting the tail vein of live mice with a dose, the highest nanoshell accumulation (approximately 12.6% of the full dose) appeared in subcutaneous tumors growing on the flanks. Similarly to the liver (∼9.2%), spleen (∼5%), kidney (∼12%), and lungs (∼8%), the clearance organs showed substantial nanoshell retentions. When comparing them with silica/gold nanoshells, hollow nanoshells have a size that is more ideal for retention and targeting.

Huang et al. [51] pioneered an in vitro study with the dual use of gold nanorods as imaging and photothermal therapeutic agents. This showed that nanorods conjugated to antibodies against the epidermal growth factor receptor (EGFR) were able to selectively target cells and cause ablation of malignant cells with half the required laser power. Another in vitro study was conducted by Goodrich et al. [159] and they reported that after 17 h of injecting the tail veins of live mice with a dose of 43.5 ± 2.3 nm gold nanorods (14 nm in radius and 45 nm in longitude), less than 10% of the total dose accumulated in subcutaneous tumors of the colon growing on the flanks, about 71% of the total injected nanorod dose accumulated in the liver, approximately 4% of the dose ended up in the spleen, and another 1% of the injected dose was found in the kidney and lymph nodes. Benefits of the smaller width of the nanorod include ease of penetration into tumors [22].

Studies on gold nanocages in PPTT were conducted by Xia et al. [32]. The use of gold nanocages was projected to be advantageous because of the structural flexibility and low power density threshold for cell death. Structures that had a diameter of 45 nm were tuned to have a SPR of 810 nm. When heated by a laser power of 1.5 W/cm^2, the viability of the isolated breast cancer cell was decreased. The use of nanocages have further been investigated for in vivo imaging [163] and photothermal treatments [164]. Imaging results showed an improved tumor uptake of the nanocages 15.3 ± 2.9% after 24 h of injection.

As found in Section 2, the hexapods can have a tunable SPR peak around 800 nm [25]. The high absorption cross section of the nanohexapod around 800 nm agrees well with its potential to serve as a photothermal reagent. A study conducted by Wang et al. [25] compared the photothermal applications of gold nanorods, gold nanocages, and gold nanohexpods by analyzing the cell uptake, biodistribution, tumor reduction, and photothermal conversion efficiencies. After 12 h of injection, gold nanohexapods exhibited the greatest cellular uptake, suggesting that branched morphology of nanostructures may lead to a higher probability of entering the cell. In addition, nanocages and nanohexapods showed great tumor reduction, ∼100% and 90% respectively. For gold nanorods, 80% tumor reduction was demonstrated after photothermal treatment. While there was no great difference in the treatment response, the use of nanohexapods demonstrated high photothermal efficiency [70]. It should also be noted that with the use of a continuous wave laser at 0.8 W/cm^2 and 808 nm, there was no change in the optical absorption of the nanostructures and no observable shift in SPR. However, upon pulsed laser irradiation of 805 nm, melting of the structures was observed at 15 mW/cm^2 for the GNR, while both nanocages and nanohexapods began melting at a pulsed laser irradiation power of 25 mW/cm^2.

Applying nanotherapeutics with magnetic fields is an exciting field for cancer therapy. Magnetic nanoparticles (MNPs) are a class of nanoparticles extensively studied and applied towards cancer therapy. These nanoparticles are used in localized thermal therapy through assistance of an external magnetic field. While pure metals with highly saturated magnetization such as Ni, Co, and Fe would serve as excellent magnetically active compounds for therapy, due to their reactive nature and cytotoxicity, their biomedical applications are limited. Therefore, compounds such as metal oxides are usually preferred as they are less sensitive to oxidation. The nanoparticles of magnetite (Fe_3O_4) and maghemite (γ-Fe_2O_3) have been extensively studied and even applied to human clinical trials for the treatment of brain cancer, glioblastoma. The first investiga-

Table 3
Clinical photothermal therapy with embedded nanoparticles.

	Dimensions (nm)	Injection dose	Targeting ligand	Tumor retention	Laser	ΔT (°C)
Nanoshell						
Au hollow [155,156]	$[R_1,R_2]$ = [–,30]	–	C225	A431, 6.8% ID/g	–	16.5
	$[R_1,R_2]$ = [40,45]	2.5×10^{12} particles	NDP-MSH	B16/F10 melanoma, 12.6% ID/g @ 4hrs	1 min, 808 nm, 0.5 W/m^2	16.5
Si–Au [52,157,158]	$[R_1,R_2]$ = [120,110]	Intratumoral, NA	–	TVT, –	4–6 min, 820 nm, 4 W/cm^2	37.4
	$[R_1,R_2]$ = [130,–]	Tail, 100 μL of 2.4×10^{11}/mL	–	CT26, –	3 min, 808 nm, 4 W/cm^2	–
	$[R_1,R_2]$ = [100,110]	Intravenous, –	–	PC-3, –	3 min, 810 nm, 4 W/cm^2	–
SPIO-Si–Au [35]	$[R_1,R_2]$ = [–,90]	Intratumoral, 100 μL, 1×10^{12} nanoparticles/mL	–	A431, 2.34% ID/g	3 min, 808 nm, 4 W/cm^2	34
Nanorod						
Au [25,159]	$[D,L]$ = [14, 45]	Tail, 4.5 ml/kg (2×10^{13} particles/mL)	–	CT26, 36 μg/g tissue	3 min, 808 nm, 1 cm tip 3.5 W	32.1
	$[D,L]$ = [9.1,36.2]	–	–	8.4% @ 24 h ID/g	10 min, 808 nm, 1.2 W/cm^2	14.5
Nanocage						
Au [25,160]	$[L,t]$ = [36.7,3.3]	Intravenous, 100 μL of 10 mg/mL	–	U87wtEGFR, 5.7% ID/g	10 min, 808 nm, 0.7 W/cm^2	–
Nanohexapod						
Au [25]	$[L,w,l]$ = [60,13.2,14.8]	Intravenous, 200 μL, 1 mg/mL	–	7.2% @ 24 h ID/g	10 min, 808 nm, 1.2 W/cm^2	23.1
Carbon nanotube						
SWNT [43,161]	$[D,L]$ = [2–5,50–300]	Intratumoral, 100 μL, 120 mg/L	–	Epidermoid KB, –	3 min, 808 nm, 76 W/cm^3	–
	$[D,L]$ = [4.3,580]	Intratumoral, 1 mg/mL	–	SCCVII, –	10 min, 785 nm, 200 mW/cm^2	15
Polymer						
PEDOTT:PSS[45]	$[D]$ = [130]	Intravenous, 200 μL, 1 mg/mL	–	4T1, 16.33% @ 24 h, 28.02% @ 48 h ID/g	5 min, 808 nm at 0.5 W/cm^2	21
Polypyrrole[77]	$[D]$ = [58]	Intravenous, 200 μL, 1 mg/mL	–	5% ID/g	5 min, 808 nm laser, at 1 W/cm^2	25

tions of using isolated magnetic nanoparticles for glioblastoma [165] and prostate cancer [166] occurred 2007 in Berlin, Germany. While MNPs were being used for glioblastoma and prostate cancer treatments, their optical properties and light to heat conversion efficiencies in in vivo did not show much flexibility. Moreover, it was difficult to tune their optical properties and red-shift their absorbance towards the NIR region.

These limitations in MNPs brought about an explosion of research in the study of metal nanoparticles such as gold, and their plasmonic effects especially in the application of nanoparticle assisted photothermal therapy. The plasmonic nature of gold, ease in bio-conjugation, simple preparation, and most importantly its strong absorptions and tunable wavelengths in the NIR region is highly attractive. While showing much promise, they continue to be limitations in tumor retention and investigators are actively searching for improvements in localization to target therapy. This has shifted recent interest towards magnetoplasmonic nanpartricles compounds that are typically nanoshells, with a core (Fe_2O_3, Fe_3O_4) surrounded by plasmonic metal shell (Ag or Au), or they can consists of a two spherical infused structures infused in a dumbell configuration with the iron oxide hybridized with the plasmonic metal [36,167]. These structures can also have a silicon layer in between the magnetic core and the metal shell [34]. Like stated in Section 2, the absorptive nature of the gold nanoshells in conjunction with the superparamagnetic properties of the core is also affected by an external magnetic field. This structure has a desirable structure that holds much potential for guided cancer therapy through a synergistic effect that includes an MRI and photothermal laser irradiation.

In 2007, Ji et al. [168] in vitro studies with a the magnetic innermost core coated with a second layer of silica between a third layer of gold were conducted. This study had a diameter between 80 and 90 nm and an average shell thickness of ~8 nm. This study was conducted at a fixed wavelength of 800 nm. As the deposition of Au on the magnetic-silica core increased, the absorbance was found to have a prominent red-shift at 800 nm. The concentration and change in temperature was linearly related up to 5.0×10^{12} particles/mL. At this time, a maximal change in temperature elevation of 16.3 °C was achieved.

Melancon et al. [35], in 2012, studied in vivo applications of the SPIO-silica\gold nanoshells. These particles, with an overall diameter of 90 nm and an outer gold shell layer of 7 nm thick, were first injected into mice with epithelial carcinoma cells. Treatment with the magnetic nanoshells and laser induced tissues resulted in significantly greater degree of necrosis: 52% compared with the saline treated tumors irradiated with laser at 18%. This study implies that changes in temperature with plasmonic magnetic nanoparticles that are guided through an MRI imaging can be mapped. Melancon and colleagues conveyed that in vivo MRI imaging provided enhanced darkening of the tumor through a comparison of a T2 map before and after SPIO gold nanoshells administration. Furthermore, it showed a decrease in signal with the presence of the multifunctional MNPs.

The process of localization is through superparamagnetic nature and alignment of magnetic fields [33], which not only helps increase cell targeting but also serves as a guidance for MRI imaging [167]. Combining an external magnetic field and a continuous wave NIR laser is advantageous because of the significantly higher localization and manipulation of the nanostructures that is achieved through the assistance of the magnetic field.

The superparamagnetic properties of the iron oxide core allows for MRI guidance and the optical characteristics of the plasmonic

outer layer to serve as a contrast agent for dark field imaging. As shown by Larson et al. [36], core/shell Fe_2O_3/Au demonstrated a drop in the T2 signal and a darkened MRI measurement that showed a significant enhancement in the MIR image comparing to the unlabeled cells. The scattering properties of the surrounding gold layer of the shell provided a reflectance cross section that conveyed a 4.5-fold greater integrated intensity than the unlabeled cells. Overall, the addition of MRI to the optical contrast of the nanoshell has the potential of guided laser therapy through obtainment of the location and concentration of the administered hybrid dosage.

4.2. Laser therapy with non-metal nanoparticles

Graphene is a novel class of nanomaterial that has great potential in biomedical applications. The first study of in vivo PPT of carbon nanomaterials with NGS conducted by Yang et al. [40], where they intravenously injected NGS and tested with mice that had different types of cancer: 4T1 murine breast cancer carcionoma and U87MG human glioblastoma. The kind of laser used was an 808 nm laser with a power of 2 W/cm^2. Since the NGS was passively targeted through intravenous delivery, the particles showed excellent tumor retention after 24 h of injection. The study by Huang et al. [43,88] was fundamental as it showed the first success of in vivo PTT with carbon nanomaterials. This is comparable to that of GNRs in terms of injected dose, administration and NIR light irradiation duration. Upon histological analysis, a high percentage of the NGS were found in the tumor and kidneys, suggesting that high renal uptake due to excretion of the smaller sized structures. Comparing to gold nanoparticles such as gold nanorods, NGS require a lower laser power for ablation, were highly efficient in passive delivery without using any targeting antibodies, and had a low percent accumulation in healthy tissues of the skin, liver, and heart.

The high electrical and thermal conductivity of CNTs have allowed the nanostructure to play a large role in the area of PTT of cancerous tumors. SWNTs not only have excellent thermal conductivity, but also are inexpensive, non-toxic through intravenous and intratumoral administration, and have a surface that can be easily coated with ligands and polymers which makes it an attractive material for nanoparticle assisted laser therapy. Huang et al. [43] investigated the effectiveness of PPT with the use of SWNTs in live clinical studies. They administered the PEG coated SWNT nanoparticles with a diameter of 4.3 nm and length of 580 nm intratumorally in mice with squamous cell carcinoma. After 5 min of injection a 785 nm diode laser with a power of 100 mW/cm^2 or 200 mW/cm^2 was used as the photoexcitation source. Ten minutes of irradiation caused an increase in temperature of 9.7–18.5 °C depending on the laser power (100 or 200 mW/cm^2) and concentration of nanoparticles administrated. The SWNTs were shown to result in ablative effects on the tumor tissue at just 200 mW/cm^2, whereas the tissue alone required 500 mW/cm^2 to achieve a comparable outcome. Comparing PTT with gold nanocages, SWNTs require lower light doses and can therefore be more advantageous in protecting healthy tissue. As noted, these structures are inexpensive, and compared to gold and polymer nanostructures they have a lower percent retention in the organs of the reticuloendothelial systems such as normal skin, liver, kidney, and heart. Although carbon based nanostructures are attractive exogenous agents for PTT, there is an incomplete understanding of the distribution, elimination, and toxicity of these materials. Also previous studies have indicated that the toxicity depends upon the administration. Some concern is SWNTs are thought to become engulfed in the outside atmosphere. For example, histological examination followed by imaging through Raman scattering showed slight accumulation of particles in lungs of both the human investigators and the mouse subjects being tested. Further investigation is warranted to determine the long term effects of localized SWNTs.

The attractive quality of most light absorbing polymers that have been tuned to the NIR region is their high photostability, a characteristic that is lacking in most of the metal nanoparticles. One of the first studies regarding the use of electrically conductive organic polymers as photothermal agents in cancer treatment was with the organic compound polyaniline [97]. Epithelial cancer cells were introduced into the mice to induce subcutaneous tumor growth in the thigh region. The polymer nanoparticles were directly injected into the tumor site and irradiated with a laser power of 2.45 W/cm^2 at a wavelength of 808 nm. Upon irradiation the tissues were examined and shown to have severe cellular and blood vessel damage when compared to the control.

Cheng et al. [45] worked to construct a nanoparticle that could serve as a novel photothermal agent for in vivo treatments. The method of delivery for their study was through intravenous injection along with the use of a fluorescent dye to measure the retention and ablative effects in subcutaneous breast cancer tumor. After 48 h, the tumor showed a high retention of particles (28.02%). While there was also significant uptake in the liver (~32%) and spleen (~16%), the particles only show toxicity when exposed to NIR light and hence only had reactivity and ablative effects in the tumors. The laser used in this study was 808 nm with a power density of 0.5 W/cm^2. The use of the polymer nanoparticle eliminated the tumor completely and the mouse remained cancer free and in good health after 45 days post treatment until sacrificed for necroscopy. Potential challenges could arise from the following observations: in vitro toxicity assessment showed that particles that were not coated with PEG coating showed dose dependent toxicity and decrease in cell viability of normal cells. This observation could cause concerns in the long term with the possibility that PEG removal could occur over time posing unforeseen side effects in areas with the highest retention rates such as the liver and spleen [45].

Studies of the polypyrrole organic nanoparticle came after the polyaniline derivatives and PEDOT:PSS experiments and pre-clinical trials [77]. These particles similarly have high photothermal conversion efficiency ~45%, are photostable, and its efficiency in thermal absorption does not decrease with time. The polypyrrole nano-polymer is also more bio-compatible than the PEDOT:PSS. No obvious sign of toxic side effects were observed.

PCPDTBT, the nanostructure described in Section 2, also shows solubility in aqueous media without the presence of a coating and has high photothermal efficiency. In the study by Macneill et al. [46], colorectal cancer cells were treated and upon just 5 min of heating, 95% of cancer cells were killed in the treatment. Although other polymers have been studied for medical applications in radiation and cancer therapy, this compound is quite unique and can eventually be preferred over other polymer nanostructures currently used for ablative treatments. The compound showed high photothermal stability when tested under repeated cycles of heating and cooling. After 48 h, the sulfur co-polymerized ligand with concentration of 62 μg-mL^{-1} also had the highest nanoparticle tumor retention. Although showing much promise, there is more work that needs to be done in order to develop into a clinically viable technology that can safely be used in patients. Future clinical testing should be studied in mice experimenting with the systemic delivery, retention rates assessment of the specific particles through the use of either MRI imaging or fluorescent dyes, and thus measurement of therapeutic thermal effects. In addition, only a small concentration of nanoparticles was required to induce cell ablation, specifically with the use of PCPDTBT.

4.3. Laser nanoparticle assisted drug delivery

Research on novel drug delivery systems with increased cell specificity and reduced adverse effects are conducted to recognize, target, and promote controlled release of drugs. Drugs can be loaded

through non-covalent interactions and covalent conjugation with either the surface coating or the metal surface of the nanoparticle. In order to select an efficient optically active delivery vehicle, one must make sure that the multifunctional system demonstrates high stability, adequate loading capacity, and is good control of size. Gene delivery focuses on treating or preventing the progression of a disease and can be used for a wide variety of ailments. Over the years, the transfer of DNA has been mediated through viral vectors [169]. Safety concerns have led to exploration of non-viral carriers including lipid [170], polymer [171], and peptide mediated delivery [172]. Characteristics for an ideal vector include non-toxic, protection from enzymatic degradation, conducive to delivery through controllable integration, and site specificity to facilitate long lasting expression. This form of therapy involves the introduction of foreign DNA into the cell and supplements or suppresses the developmental expression of a malignant cell. Gene delivery has been used for the treatment of immunodeficieny, neovascular disorders such as retinopathy, age related macular degeneration, HIV, cancer, and various other complex diseases [173].

Photothermal release of drugs from gold nanoparticles is a mature, facile, and straightforward application of cancer therapy that allows for multifunctional thermal treatment. In 2000, Sershen and Westcott [93] were one of the first investigators to study the effects of combined plasmonic nanoshell delivery of drug molecules through laser irradiation. The controlled release of drugs can be modulated through temperature sensitive hydrogels and optically active polymer gold nanoshell composites. They studied gold nanoshells with a 37 nm diameter gold sulfide core and a gold shell thickness of 4 nm infused within a hydrogel mixed and stabilized with drugs ovalbumin and bovine serum albumin (BSA). The flexibility and tunable nature of nanoparticles holds an advantage in serving as carrier for both drug and gene delivery. CNTs are widely used as drug and gene delivery agents as well.

5. Conclusion

The collective efforts of biologists, physicists, engineers and clinicians committed to advancing thermal medicine will lead towards many paths that improve cancer therapies. The scientists have designed metal and non-metal nanoparticles of various shapes, sizes, and material in order to find the best tunable nanoparticles that will be ideal for photothermal therapies. Both experimental and numerical tests have been conducted in order to further understand the consequences of nanoparticle assisted thermal heating.

Prior to administering and conducting clinically trials on human subjects it is important to study the cytotoxic effects of such particles. Since the safety of metal nanoparticles is not completely assessed and has sparked concerns in the general population, especially with the kind of coatings used to increase solubility in the circulation system, one should study these effects further in detail. Another issue is the thermophysicial properties of these particles that were presented in Section 2. When heating, these nanoparticles can develop a nanobubble, or vapor bubble, surrounding the particle. The issue of how these nanoparticles may deform as a consequence of heating and therefore may alter the optical properties is unresolved. More optimization of how long the laser should be directed at the nanoparticle induced laser or how many lasers are to be used still needs to be studied. Nanoparticle assisted laser treatment has the potential to beat cancer once it is further researched.

Acknowledgments

Thanks to Alliances for Graduate Education and the Professoriate (AGEP) and Dr. Bayazitoglu's heat transfer lab at Rice University for their contribution. This work is supported by NSF Cooperative Agreement Number HRD-0450363 and John and Ann Doerr Fund for Computational Biomedicine.

References

[1] H.P. Liang, L.J. Wan, C.L. Bai, L. Jiang, Gold hollow nanospheres: tunable surface plasmon resonance controlled by interior cavity sizes, J. Phys. Chem. B 109 (16) (2005) 7795–7800.
[2] S. Berber, Y.K. Kwon, D. Tománek, Unusually high thermal conductivity of carbon nanotubes, Phys. Rev. Lett. 84 (20) (2000) 4613–4616.
[3] T.W. Ebbesen, H.J. Lezec, H. Hiura, J.W. Bennett, H.F. Ghaemi, T. Thio, Electrical conductivity of individual carbon nanotubes, Nature 382 (6586) (1996) 54–56.
[4] Z. Yao, C. Kane, C. Dekker, High field electrical transport in single-wall carbon nanotubes, Phys. Rev. Lett. 84 (13) (2000) 2941–2944.
[5] F. Duck, Physical Properties of Tissue: A Comprehensive Reference Book, Academic Press, London, 1990.
[6] W.F. Cheong, S.A. Prahl, A.J. Welch, A review of the optical properties of biological tissues, IEEE J. Quantum Electron. 26 (12) (1990) 2166–2185.
[7] I.H. El-Sayed, X. Huang, M.A. El-Sayed, Selective laser photothermal therapy of epithelial carcinoma using anti-EGFR antibody conjugated gold nanoparticles, Cancer Lett. 239 (1) (2006) 129–135.
[8] H.C. van de Hulst, Light Scattering by Small Particles, John Wiley & Sons, Inc., New York, 1957.
[9] C.F. Bohren, D.R. Huffman, Absorption and Scattering of Light by Small Particles, Wiley-VCH Verlag GmbH, New York, 1983.
[10] M. Hu, J. Chen, Z.Y. Li, L. Au, G.V. Hartland, X. Li, M. Marquez, Y. Xia, Gold nanostructures: engineering their plasmonic properties for biomedical applications, Chem. Soc. Rev. 35 (11) (2006) 1084–1094.
[11] B. Khlebtsov, V. Zharov, A. Melnikov, V. Tuchin, N. Khlebtsov, Optical amplification of photothermal therapy with gold nanoparticles and nanoclusters, Nanotechnology 17 (20) (2006) 5167–5179.
[12] P.K. Jain, K.S. Lee, I.H. El-Sayed, M.A. El-Sayed, Calculated absorption and scattering properties of gold nanoparticles of different size, shape, and composition: applications in biological imaging and biomedicine, J. Phys. Chem. B 110 (14) (2006) 7238–7248.
[13] V. Myroshnychenko, J. Rodríguez-Fernández, I. Pastoriza-Santos, A.M. Funston, C. Novo, P. Mulvaney, L.M. Liz-Marzán, F.J. García de Abajo, Modelling the optical response of gold nanoparticles, Chem. Soc. Rev. 37 (9) (2008) 1792–1805.
[14] S. Kessentini, D. Barchiesi, Quantitative comparison of optimized nanorods, nanoshells and hollow nanospheres for photothermal therapy, Biomed. Opt. Express 3 (3) (2012) 590–604.
[15] P.K. Jain, I.H. El-Sayed, M.A. El-Sayed, Au nanoparticles target cancer, Nano Today 2 (1) (2007) 18–29.
[16] X. Huang, P.K. Jain, I.H. El-Sayed, M.A. El-Sayed, Plasmonic photothermal therapy (PPTT) using gold nanoparticles, Lasers Med. Sci. 23 (3) (2008) 217–228.
[17] P.K. Jain, X. Huang, I.H. El-Sayed, M.A. El-Sayed, Noble metals on the nanoscale: optical and photothermal properties and some applications in imaging, sensing, biology, and medicine, Acc. Chem. Res. 41 (12) (2008) 1578–1586.
[18] X. Huang, M.A. El-Sayed, Gold nanoparticles: optical properties and implementations in cancer diagnosis and photothermal therapy, J. Adv. Res. 1 (1) (2010) 13–28.
[19] E.C. Dreaden, M.A. Mackey, X. Huang, B. Kang, M.A. El-Sayed, Beating cancer in multiple ways using nanogold, Chem. Soc. Rev. 40 (7) (2011) 3391–3404.
[20] J.K. Young, E.R. Figueroa, R.A. Drezek, Tunable nanostructures as photothermal theranostic agents, Ann. Biomed. Eng. 40 (2) (2012) 438–459.
[21] E.S. Day, J.G. Morton, J.L. West, Nanoparticles for thermal cancer therapy, J. Biomech. Eng. 131 (7) (2009).
[22] L.C. Kennedy, L.R. Bickford, N.A. Lewinski, A.J. Coughlin, Y. Hu, E.S. Day, J.L. West, R.A. Drezek, A new era for cancer treatment: gold-nanoparticle-mediated thermal therapies, Small 7 (2) (2011) 69–83.
[23] Z. Qin, J.C. Bischof, Thermophysical and biological responses of gold nanoparticle laser heating, Chem. Soc. Rev. 41 (3) (2012) 1191–1217.
[24] G. Baffou, R. Quidant, Thermo-plasmonics: using metallic nanostructures as nano-sources of heat, Laser Photonics Rev. 7 (2) (2013) 171–187.
[25] Y. Wang, K.C.L. Black, H. Luehmann, W. Li, Y. Zhang, X. Cai, D. Wan, S.-Y. Liu, M. Li, P. Kim, Z.-Y. Li, L.V. Wang, Y. Liu, Y. Xia, Comparison study of gold nanohexapods, nanorods, and nanocages for photothermal cancer treatment, ACS Nano 7 (3) (2013) 2068–2077.
[26] T.A. Erickson, J.W. Tunnell, Gold Nanoshells in Biomedical Applications, Nanotechnologies for the Life Sciences, Wiley-VCH Verlag GmbH & Co. KGaA, 2010.
[27] R. Bardhan, S. Lal, A. Joshi, N.J. Halas, Theranostic nanoshells: from probe design to imaging and treatment of cancer, Acc. Chem. Res. 44 (10) (2011) 936–946.
[28] X. Huang, S. Neretina, M.A. El-Sayed, Gold nanorods: from synthesis and properties to biological and biomedical applications, Adv. Mater. 21 (48) (2009) 4880–4910.
[29] T. Zhang, C. Li, L. Zhao, Y. Ren, G. Moran, X. Zhang, H. Cai, Progress in cancer diagnosis and treatment based on gold nanorods, in: 2010 International

Conference on Manipulation, Manufacturing, and Measurement on the Nanoscale (3M-NAN)), 2012, pp. 425–430.
[30] W.I. Choi, A. Sahu, Y.H. Kim, G. Tae, Photothermal cancer therapy and imaging based on gold nanorods., Ann. Biomed. Eng. 40 (2) (2012) 534–546.
[31] Z. Zhang, J. Wang, C. Chen, Gold nanorods based platforms for light-mediated theranostics, Theranostics 3 (3) (2013) 223–238.
[32] Y. Xia, C.M. Cobley, L. Au, X. Lu, Y. Sun, J. Chen, S.E. Skrabalak, Gold nanocages: synthesis, properties, and applications, Acc. Chem. Res. 41 (12) (2008) 1587–1595.
[33] A. Sarychev, G. Shvets, V. Shalaev, Magnetic plasmon resonance, Phys. Rev. E 73 (3) (2006).
[34] M.A. Correa-Duarte, M. Farle, A. Lo, K. Sieradzki, R. Diaz, Bifunctional gold-coated magnetic silica spheres, Chem. Matters 18 (11) (2006) 2701–2706.
[35] M.P. Melancon, A. Elliott, X. Ji, A. Shetty, Z. Yang, M. Tian, B. Taylor, R.J. Stafford, C. Li, Theranostics with multifunctional magnetic gold nanoshells: photothermal therapy and T2* magnetic resonance imaging, Invest. Radiol. 46 (2) (2011) 132–140.
[36] T.A. Larson, J. Bankson, J. Aaron, K. Sokolov, Hybrid plasmonic magnetic nanoparticles as molecular specific agents for MRI/optical imaging and photothermal therapy of cancer cells, Nanotechnology 18 (32) (2007) 325101.
[37] D.D. Evanoff, G. Chumanov, Synthesis and optical properties of silver nanoparticles and arrays, Chem. Phys. Chem. 6 (7) (2005) 1221–1231.
[38] S.C. Boca, M. Potara, A.-M. Gabudean, A. Juhem, P.L. Baldeck, S. Astilean, Chitosan-coated triangular silver nanoparticles as a novel class of biocompatible, highly effective photothermal transducers for in vitro cancer cell therapy, Cancer Lett. 311 (2) (2011) 131–140.
[39] I. Sur, D. Cam, M. Kahraman, A. Baysal, M. Culha, Interaction of multi-functional silver nanoparticles with living cells, Nanotechnology 21 (17) (2010) 175104.
[40] K. Yang, S. Zhang, G. Zhang, X. Sun, S.T. Lee, Z. Liu, Graphene in mice: ultrahigh in vivo tumor uptake and efficient photothermal therapy, Nano Lett. 10 (9) (2010) 3318–3323.
[41] C. Fisher, A.E. Rider, Z. Jun Han, S. Kumar, I. Levchenko, K. Ostrikov, Applications and nanotoxicity of carbon nanotubes and graphene in biomedicine, J. Nanomater. (2012) 1–19.
[42] F. Zhou, D. Xing, Z. Ou, B. Wu, D.E. Resasco, W.R. Chen, Cancer photothermal therapy in the near-infrared region by using single-walled carbon nanotubes, J. Biomed. Opt. 14 (2) (2009). 021009.
[43] N. Huang, H. Wang, J. Zhao, H. Lui, M. Korbelik, H. Zeng, Single-wall carbon nanotubes assisted photothermal cancer therapy: animal study with a murine model of squamous cell carcinoma, Lasers Surg. Med. 42 (9) (2010) 638–648.
[44] J.W. Fisher, S. Sarkar, C.F. Buchanan, C.S. Szot, J. Whitney, H.C. Hatcher, S.V. Torti, C.G. Rylander, M.N. Rylander, Photothermal response of human and murine cancer cells to multiwalled carbon nanotubes after laser irradiation, Cancer Res. 70 (23) (2010) 9855–9864.
[45] L. Cheng, K. Yang, Q. Chen, Z. Liu, Organic stealth nanoparticles for highly effective in vivo near-infrared photothermal therapy of cancer, ACS Nano 6 (6) (2012) 5605–5613.
[46] C.M. Macneill, R.C. Coffin, D.L. Carroll, N.H. Levi-Polyachenko, Low band gap donor–acceptor conjugated polymer nanoparticles and their NIR-mediated thermal ablation of cancer cells, Macromol. Biosci. 13 (2013) 28–34.
[47] N. Kamaly, Z. Xiao, P.M. Valencia, A.F. Radovic-Moreno, O.C. Farokhzad, Targeted polymeric therapeutic nanoparticles: design, development and clinical translation, Chem. Soc. Rev. 41 (7) (2012) 2971–3010.
[48] N.G. Khlebtsov, L.A. Dykman, Optical properties and biomedical applications of plasmonic nanoparticles, J. Quant. Spectrosc. Radiat. Transfer 111 (1) (2010) 1–35.
[49] I. Pastoriza-Santos, D. Gomez, J. Perez-Juste, L. Liz-Marzan, P. Mulvaney, Optical properties of metal nanoparticle coated silica spheres: a simple effective medium approach, Phys. Chem. Chem. Phys. 6 (2004) 5056–5060.
[50] M. Hu, G.V. Hartland, Heat dissipation for Au particles in aqueous solution: relaxation time versus size, J. Phys. Chem. B 106 (28) (2002) 7029–7033.
[51] X. Huang, I.H. El-Sayed, W. Qian, M.A. El-Sayed, Cancer cell imaging and photothermal therapy in the near-infrared region by using gold nanorods, J. Am. Chem. Soc. 128 (6) (2006) 2115–2120.
[52] D.P. O'Neal, L.R. Hirsch, N.J. Halas, J.D. Payne, J.L. West, Photo-thermal tumor ablation in mice using near infrared-absorbing nanoparticles, Cancer Lett. 209 (2) (2004) 171–176.
[53] D. Lapotko, Plasmonic nanoparticle-generated photothermal bubbles and their biomedical applications, Nanomedicine 4 (7) (2009) 813–845.
[54] T.B. Huff, L. Tong, Y. Zhao, M.N. Hansen, J.X. Cheng, A. Wei, Hyperthermic effects of gold nanorods on tumor cells, Nanomedicine 2 (1) (2007) 125–132.
[55] E.Y. Lukianova-Hleb, M.B.G. Mutonga, D.O. Lapotko, Cell-specific multifunctional processing of heterogeneous cell systems in a single laser pulse treatment., ACS Nano 6 (12) (2012) 10973–10981.
[56] V.P. Zharov, R.R. Letfullin, E.N. Galitovskaya, Microbubbles-overlapping mode for laser killing of cancer cells with absorbing nanoparticle clusters, J. Phys. D Appl. Phys. 38 (15) (2005) 2571–2581.
[57] D. Lapotko, Optical excitation and detection of vapor bubbles around plasmonic nanoparticles, Opt. Express 17 (4) (2009) 2538–2556.
[58] V.K. Pustovalov, A.S. Smetannikov, V.P. Zharov, Photothermal and accompanied phenomena of selective nanophotothermolysis with gold nanoparticles and laser pulses, Laser Phys. Lett. 5 (11) (2008) 775–792.
[59] E.Y. Lukianova-Hleb, E. Sassaroli, A. Jones, D.O. Lapotko, Transient photothermal spectra of plasmonic nanobubbles, Langmuir: ACS J. Surf. Colloids 28 (10) (2012) 4858–4866.
[60] V.P. Zharov, Ultrasharp nonlinear photothermal and photoacoustic resonances and holes beyond the spectral limit, Nat. Photonics 5 (2011) 110–116.
[61] E. Boulais, R. Lachaine, M. Meunier, Plasma mediated off-resonance plasmonic enhanced ultrafast laser-induced nanocavitation, Nano Lett. 12 (9) (2012) 4763–4769.
[62] E. Boulais, R. Lachaine, M. Meunier, Basic mechanisms of the femtosecond laser interaction with a plasmonic nanostructure in water, in: Frontiers in Ultrafast Optics:Biomedical, Scientific, and Industrial Applications, vol. 7925, 2011, p. 79250G–5.
[63] A.O. Govorov, H.H. Richardson, Generating heat with metal nanoparticles, Nano Today 2 (1) (2007) 30–38.
[64] Y. Bayazitoglu, S. Kheradmand, T.K. Tullius, Thermal therapy with metal nanoparticle assisted laser heating, in: Proceedings of the Seventh International Symposium on Radiative Transfer, Kuşadasi, Turkey RAD-13-D1, 2013.
[65] J.A. Edgar, H.M. Zareie, M. Blaber, A. Dowd, M.B. Cortie, Synthesis of hollow gold nanoparticles and rings using silver templates, in: 2008 International Conference on Nanoscience and, Nanotechnology, 2008, pp. 36–39.
[66] J.R. Cole, N.J. Halas, Optimized plasmonic nanoparticle distributions for solar spectrum harvesting, Appl. Phys. Lett. 89 (15) (2006).
[67] P. Tuersun, X. Han, Optical absorption analysis and optimization of gold nanoshells, Appl. Opt. 52 (6) (2013) 1325–1329.
[68] J. Chen, F. Saeki, B.J. Wiley, H. Cang, M.J. Cobb, Z.Y. Li, L. Au, H. Zhang, M.B. Kimmey, X. Li, Y. Xia, Gold nanocages: bioconjugation and their potential use as optical imaging contrast agents, Nano Lett. 5 (3) (2005) 473–477.
[69] L.J.E. Anderson, C.M. Payne, Y.R. Zhen, P. Nordlander, J.H. Hafner, A tunable plasmon resonance in gold nanobelts, Nano Lett. 11 (11) (2011) 5034–5037.
[70] D.Y. Kim, T. Yu, E.C. Cho, Y. Ma, O.O. Park, Y. Xia, Synthesis of gold nano-hexapods with controllable arm lengths and their tunable optical properties, Angew. Chem. Int. Ed. Engl. 50 (28) (2011) 6328–6331.
[71] S.J. Oldenburg, S.L. Westcott, R.D. Averitt, N.J. Halas, Surface enhanced Raman scattering in the near infrared using metal nanoshell substrates, J. Chem. Phys. 111 (10) (1999).
[72] C. Loo, A. Lin, L. Hirsch, M.H. Lee, J. Barton, N. Halas, J. West, R. Drezek, Nanoshell-enabled photonics-based imaging and therapy of cancer, Technol. Cancer Res. Treat. 3 (1) (2004) 33–40.
[73] A.M. Schwartzberg, T.Y. Olson, C.E. Talley, J.Z. Zhang, Synthesis, characterization, and tunable optical properties of hollow gold nanospheres, J. Phys. Chem. B 110 (40) (2006) 19935–19944.
[74] S.S. Chang, C.W. Shih, C.D. Chen, W.C. Lai, C.R.C. Wang, The shape transition of gold nanorods, Langmuir 15 (3) (1999) 701–709.
[75] S. Link, C. Burda, B. Nikoobakht, M.a. El-Sayed, Laser-induced shape changes of colloidal gold nanorods using femtosecond and nanosecond laser pulses, J. Phys. Chem. B 104 (26) (2000) 6152–6163.
[76] Z.L. Wang, Nanowires and Nanobelts: Materials, Properties and Devices, Springer, US, Boston, MA, 2003.
[77] M. Chen, X. Fang, S. Tang, N. Zheng, Polypyrrole nanoparticles for high-performance in vivo near-infrared photothermal cancer therapy, Chem. Commun. 48 (71) (2012) 8934–8936.
[78] W.A. El-Said, C.H. Yea, J.W. Choi, I.K. Kwon, Ultrathin polyaniline film coated on an indium–tin oxide cell-based chip for study of anticancer effect, Thin Solid Films 518 (2) (2009) 661–667.
[79] X. Li, X. Wang, L. Zhang, S. Lee, H. Dai, Chemically derived, ultrasmooth graphene nanoribbon semiconductors, Science 319 (5867) (2008) 1229–1232.
[80] L. Jiao, L. Zhang, X. Wang, G. Diankov, H. Dai, Narrow graphene nanoribbons from carbon nanotubes, Nature 458 (7240) (2009) 877–880.
[81] L. Feng, Z. Liu, Graphene in biomedicine: opportunities and challenges, Nanomedicine 6 (2) (2011) 317–324.
[82] K. Yang, L. Feng, X. Shi, Z. Liu, Nano-graphene in biomedicine: theranostic applications, Chem. Soc. Rev. 42 (2) (2013) 530–547.
[83] R.H. Baughman, A.A. Zakhidov, W.A. de Heer, Carbon nanotubes-the route toward applications, Science 297 (5582) (2002) 787–792.
[84] V.N. Khabashesku, J.L. Margrave, E.V. Barrera, Functionalized carbon nanotubes and nanodiamonds for engineering and biomedical applications, Diamond Relat. Mater. 14 (3–7) (2005) 859–866.
[85] S. Polizu, O. Savadogo, P. Poulin, L. Yahia, Applications of carbon nanotubes-based biomaterials in biomedical nanotechnology, J. Nanosci. Nanotechnol. 6 (7) (2006) 1883–1904.
[86] G. Cellot, E. Cilia, S. Cipollone, V. Rancic, A. Sucapane, S. Giordani, L. Gambazzi, H. Markram, M. Grandolfo, D. Scaini, F. Gelain, L. Casalis, M. Prato, M. Giugliano, L. Ballerini, Carbon nanotubes might improve neuronal performance by favouring electrical shortcuts, Nat. Nanotechnol. 4 (2) (2009) 126–133.
[87] Z. Liu, S. Tabakman, K. Welsher, H. Dai, Carbon nanotubes in biology and medicine: in vitro and in vivo detection, imaging and drug delivery, Nano Res. 2 (2) (2009) 85–120.
[88] N. Huang, H. Wang, J. Zhao, H. Lui, M. Korbelik, H. Zeng, Carbon nanotube assisted photothermal therapy of skin cancers-pilot proof-of-principle study in a murine model, Proceedings of SPIE 7548, Photonic Therapeutics and Diagnostics VI, 2010, 75480H–3.

[89] D. Peer, J.M. Karp, S. Hong, O.C. Farokhzad, R. Margalit, R. Langer, Nanocarriers as an emerging platform for cancer therapy, Nat. Nanotechnol. 2 (12) (2007) 751–760.
[90] R. Singh, J.W. Lillard, Nanoparticle-based targeted drug delivery, Exp. Mol. Pathol. 86 (3) (2009) 215–223.
[91] T. Niidome, L. Huang, Gene therapy progress and prospects: nonviral vectors, Gene Ther. 9 (24) (2002) 1647–1652.
[92] K. Yang, H. Xu, L. Cheng, C. Sun, J. Wang, Z. Liu, In vitro and in vivo near-infrared photothermal therapy of cancer using polypyrrole organic nanoparticles, Adv. Mater. 24 (41) (2012) 5586–5592 (Deerfield Beach, Fla.).
[93] S. Sershen, S. Westcott, Temperature sensitive polymer–nanoshell composites for photothermally modulated drug delivery, J. Biomed. Mater. Res. 51 (3) (2000) 293–298.
[94] B. Sahoo, K.S.P. Devi, R. Banerjee, T.K. Maiti, P. Pramanik, D. Dhara, Thermal and pH responsive polymer-tethered multifunctional magnetic nanoparticles for targeted delivery of anti-cancer drug, ACS Appl. Mater. Interfaces 5 (9) (2013) 3884–3893.
[95] J.U. Menon, P. Jadeja, P. Tambe, K. Vu, B. Yuan, K.T. Nguyen, Nanomaterials for photo-based diagnostic and therapeutic applications, Theranostics 3 (3) (2013) 152–166.
[96] G.L. Gibson, T.M. McCormick, D.S. Seferos, Atomistic band gap engineering in donor–acceptor polymers, J. Am. Chem. Soc. 134 (1) (2012) 539–547.
[97] J. Yang, J. Choi, D. Bang, E. Kim, E.K. Lim, H. Park, J.S. Suh, K. Lee, K.H. Yoo, E.K. Kim, Y.M. Huh, S. Haam, Convertible organic nanoparticles for near-infrared photothermal ablation of cancer cells, Angew. Chem. Int. Ed. Engl. 50 (2) (2011) 441–444.
[98] X. Xu, A. Meade, Y. Bayazitoglu, Numerical investigation of nanoparticle-assisted laser-induced interstitial thermotherapy toward tumor and cancer treatments, Lasers Med. Sci. 26 (2) (2011) 213–222.
[99] L.A. Dombrovsky, V. Timchenko, M. Jackson, G.H. Yeoh, A combined transient thermal model for laser hyperthermia of tumors with embedded gold nanoshells, Int. J. Heat Mass Transfer 54 (25–26) (2011) 5459–5469.
[100] P. Diagaradjane, A. Shetty, J.C. Wang, A.M. Elliott, J. Schwartz, S. Shentu, H.C. Park, A. Deorukhkar, R.J. Stafford, S.H. Cho, J.W. Tunnell, J.D. Hazle, S. Krishnan, Modulation of in vivo tumor radiation response via gold nanoshell-mediated vascular-focused hyperthermia: characterizing an integrated antihypoxic and localized vascular disrupting targeting strategy, Nano Lett. 8 (5) (2008) 1492–1500.
[101] J. Parsons, C.P. Burrows, J.R. Sambles, W.L. Barnes, A comparison of techniques used to simulate the scattering of electromagnetic radiation by metallic nanostructures, J. Mod. Opt. 57 (5) (2010) 356–365.
[102] C. Matzler, MATLAB functions for Mie scattering and absorption, Institute of Applied Physics, University of Bern, 2002 (Online). Available: http://arrc.ou.edu/~rockee/NRA_2007_website/Mie-scattering-Matlab.pdf. [Accessed: 20-Jun-2013].
[103] G. Mie, Beiträge zur Optik trüber Medien, speziell kolloidaler Metallösungen, Ann. Phys. 330 (3) (1908) 377–445.
[104] V.L.Y. Loke, M. Pinar Mengüç, T.A. Nieminen, Discrete-dipole approximation with surface interaction: computational toolbox for MATLAB, J. Quant. Spectrosc. Radiat. Transfer 112 (11) (2011) 1711–1725.
[105] E.M. Purcell, C.R. Pennypacker, Scattering and absorption of light by nonspherical dielectric grains, Astrophys. J. 186 (1973) 705.
[106] B.T. Draine, P.J. Flatau, Discrete-dipole approximation for scattering calculations, J. Opt. Soc. Am. 11 (4) (1994) 1491–1499.
[107] F.J. Garcıa de Abajo, A. Howie, Retarded field calculation of electron energy loss in inhomogeneous dielectrics, Phys. Rev. B 65 (2002).
[108] C. Oubre, P. Nordlander, Finite-difference time-domain studies of the optical properties of nanoshell dimers, J. Phys. Chem. B 109 (20) (2005) 10042–10051.
[109] F. Hao, C.L. Nehl, J.H. Hafner, P. Nordlander, Plasmon resonances of a gold nanostar, Nano Lett. 7 (3) (2007) 729–732.
[110] Z. Zhang, Nano/Microscale Heat Transfer, McGraw-Hill Professional, 2007.
[111] C.D. Mobley, L.K. Sundman, Hydrolight 4.2 technical documentation, Sequoia Scientific, Inc., Westpark Technical Center, 2001.
[112] B.T. Draine, P.J. Flatau, User guide for the discrete dipole approximation code DDSCAT 7.2, p. 95, 2012 (Online). Available: http://arxiv.org/abs/1202.3424. (Accessed: 25-Jun-2013).
[113] A.M. Gobin, M.H. Lee, N.J. Halas, W.D. James, R.a. Drezek, J.L. West, Near-infrared resonant nanoshells for combined optical imaging and photothermal cancer therapy, Nano Lett. 7 (7) (2007) 1929–1934.
[114] C.M. Chu, S.W. Churchill, Representation of the angular distribution of radiation scattered by a spherical particle, J. Opt. Soc. Am. 45 (11) (1955) 958.
[115] G.C. Clark, C.M. Chu, S.W. Churchill, Angular distribution coefficients for radiation scattered by a spherical particle, J. Opt. Soc. Am. 47 (1) (1957).
[116] M.F Modest, Radiative Heat Transfer, second ed., Academic Press, 2003.
[117] L.A. Dombrovsky, V. Timchenko, M. Jackson, Indirect heating strategy for laser induced hyperthermia: an advanced thermal model, Int. J. Heat Mass Transfer 55 (17–18) (2012) 4688–4700.
[118] L.A. Dombrovsky, The use of transport approximation and diffusion-based models in radiative transfer calculations, Comput. Therm. Sci. 4 (4) (2012) 297–315.
[119] A.M. Elliott, J. Schwartz, J. Wang, A.M. Shetty, C. Bourgoyne, D.P. O'Neal, J.D. Hazle, R.J. Stafford, Quantitative comparison of delta P1 versus optical diffusion approximations for modeling near-infrared gold nanoshell heating, Med. Phys. 36 (4) (2009) 1351–1358.
[120] J. Vera, Y. Bayazitoglu, A note on laser penetration in nanoshell deposited tissue, Int. J. Heat Mass Transfer 52 (13–14) (2009) 3402–3406.
[121] J. Vera, Y. Bayazitoglu, Gold nanoshell density variation with laser power for induced hyperthermia, Int. J. Heat Mass Transfer 52 (3–4) (2009) 564–573.
[122] I.K. Tjahjono, Y. Bayazitoglu, Near-infrared light heating of a slab by embedded nanoparticles, Int. J. Heat Mass Transfer 51 (7–8) (2008) 1505–1515.
[123] S.A. Carp, S.A. Prahl, V. Venugopalan, Radiative transport in the delta-P1 approximation: accuracy of fluence rate and optical penetration depth predictions in turbid semi-infinite media, J. Biomed. Opt. 9 (3) (2004) 632–647.
[124] I. Seo, C.K. Hayakawa, V. Venugopalan, Radiative transport in the delta-P1 approximation for semi-infinite turbid media, Med. Phys. 35 (2) (2008) 681–693.
[125] D. Fuentes, J.T. Oden, K.R. Diller, J.D. Hazle, A. Elliott, A. Shetty, R.J. Stafford, Computational modeling and real-time control of patient-specific laser treatment of cancer, Ann. Biomed. Eng. 37 (4) (2009) 763–782.
[126] L. Wang, S.L. Jacques, L. Zheng, MCML-Monte Carlo modeling of light transport in multi-layered tissues, Comput. Methods Programs Biomed. 47 (2) (1995) 131–146.
[127] A.J. Welch, C.M. Gardner, Monte Carlo model for determination of the role of heat generation in laser-irradiated tissue, J. Biomech. Eng. 119 (4) (1997) 489–495.
[128] M.L. De Jode, Monte Carlo simulations of light distributions in an embedded tumour model: studies of selectivity in photodynamic therapy, Lasers Med. Sci. 15 (1) (2000) 49–56.
[129] A.W.H. Lin, N.A. Lewinski, J.L. West, N.J. Halas, R.A. Drezek, Optically tunable nanoparticle contrast agents for early cancer detection: model-based analysis of gold nanoshells, J. Biomed. Opt. 10 (6) (2005).
[130] Y. Feng, D. Fuentes, A. Hawkins, J. Bass, M.N. Rylander, A. Elliott, A. Shetty, R.J. Stafford, J.T. Oden, Nanoshell-mediated laser surgery simulation for prostate cancer treatment, Eng. Comput. 25 (1) (2009) 3–13.
[131] Y. Feng, D. Fuentes, Model-based planning and real-time predictive control for laser-induced thermal therapy, Int. J. Hyperthermia 27 (8) (2011) 751–761.
[132] T. Grosges, D. Barchiesi, S. Kessentini, G. Gréhan, M.L. de la Chapelle, Nanoshells for photothermal therapy: a Monte-Carlo based numerical study of their design tolerance, Biomed. Opt. Express 2 (6) (2011) 1584–1596.
[133] X. Xu, A. Meade, Y. Bayazitoglu, Feasibility of selective nanoparticle-assisted photothermal treatment for an embedded liver tumor, Lasers Med. Sci. (2012).
[134] M.N.R.Y. Feng, Y. Feng, M.N. Rylander, J. Bass, J.T. Oden, K. Diller, Optimal design of laser surgery for cancer treatment through nanoparticle-mediated hyperthermia therapy, NSTI-Nanotech 1 (2005) 39–42.
[135] M. Kirillin, M. Shirmanova, M. Sirotkina, M. Bugrova, B. Khlebtsov, E. Zagaynova, Contrasting properties of gold nanoshells and titanium dioxide nanoparticles for optical coherence tomography imaging of skin: Monte Carlo simulations and in vivo study, J. Biomed. Opt. 14 (2) (2009).
[136] S. Wang, C.W. Lee, A. Chiou, P.K. Wei, Size-dependent endocytosis of gold nanoparticles studied by three-dimensional mapping of plasmonic scattering images, J. Nanobiotechnol. 8 (1) (2010) 33.
[137] S.D. Perrault, C. Walkey, T. Jennings, H.C. Fischer, W.C.W. Chan, Mediating tumor targeting efficiency of nanoparticles through design, Nano Lett. 9 (5) (2009) 1909–1915.
[138] S.K. Balasubramanian, J. Jittiwat, J. Manikandan, C.N. Ong, L.E. Yu, W.Y. Ong, Biodistribution of gold nanoparticles and gene expression changes in the liver and spleen after intravenous administration in rats, Biomaterials 31 (8) (2010) 2034–2042.
[139] M.A. Dobrovolskaia, A.K. Patri, J. Zheng, J.D. Clogston, N. Ayub, P. Aggarwal, B.W. Neun, J.B. Hall, S.E. McNeil, Interaction of colloidal gold nanoparticles with human blood: effects on particle size and analysis of plasma protein binding profiles, Nanomed. Nanotech. Biol. Med. 5 (2) (2009) 106–117.
[140] H.H. Pennes, Analysis of tissue and arterial blood temperatures in the resting human forearm, J. Appl. Physiol. 1 (2) (1948) 93–122.
[141] E.H. Wissler, 'Pennes' 1948 paper revisited, J. Appl. Physiol. 85 (1) (1998) 35–41.
[142] A. Nakayama, F. Kuwahara, A general bioheat transfer model based on the theory of porous media, Int. J. Heat Mass Transfer 51 (11–12) (2008) 3190–3199.
[143] Y. Bayazitoglu, Nanoshell assisted cancer therapy: numerical simulations, in: ASME 2009 Second International Conference on Micro/Nanoscale Heat and Mass Transfer, vol. 3, pp. 545–552, 2009.
[144] G.J. Müller, A. Roggan, Interstitial laser hyperthermia – a new method to treat tumors, Laser-Induced Interstitial Thermotherapy, SPIE Publications, 1992.
[145] B. Gewiese, J. Beuthan, F. Fobbe, D. Stiller, G. Müller, J. Böse-Landgraf, K.J. Wolf, M. Deimling, Magnetic resonance imaging-controlled laser-induced interstitial thermotherapy, Invest. Radiol. 29 (3) (1994) 345–351.
[146] G. Muller, A. Roggan, Laser-Induced Interstitial Thermotherapy, SPIE Optical Engineering Press, Bellingham, 1995.
[147] Laser therapy offers alternative to surgery for liver tumors, Medical Devices & Surgical Technology Week NewsRX HighBeam Research, 2003 [Online]. Available: http://www.newsrx.com/newsletters/Medical-Devices-and-Surgical-Technology-Week/2003-10-12/1012200333332QW.html.
[148] A. Elliott, J. Schwartz, J. Wang, A. Shetty, J. Hazle, J.R. Stafford, Analytical solution to heat equation with magnetic resonance experimental verification

for nanoshell enhanced thermal therapy, Lasers Surg. Med. 40 (9) (2008) 660–665.
[149] S.H. Cho, Estimation of tumour dose enhancement due to gold nanoparticles during typical radiation treatments: a preliminary Monte Carlo study, Phys. Med. Biol. 50 (15) (2005) N163–N173.
[150] S. Banerjee, S.K. Sharma, Use of Monte Carlo simulations for propagation of light in biomedical tissues, Appl. Opt. 49 (22) (2010).
[151] A. Kienle, M.S. Patterson, Improved solutions of the steady-state and the time-resolved diffusion equations for reflectance from a semi-infinite turbid medium, J. Opt. Soc. Am. A 14 (1) (1997) 246.
[152] D. Contini, F. Martelli, G. Zaccanti, Photon migration through a turbid slab described by a model based on diffusion approximation. I. Theory, Appl. Opt. 36 (19) (1997) 4587.
[153] A. Fasano, D. Hömberg, D. Naumov, On a mathematical model for laser-induced thermotherapy, Appl. Math. Model. 34 (12) (2010) 3831–3840.
[154] J.A. Schwartz, A.M. Shetty, R.E. Price, R.J. Stafford, J.C. Wang, R.K. Uthamanthil, K. Pham, R.J. McNichols, C.L. Coleman, J.D. Payne, Feasibility study of particle-assisted laser ablation of brain tumors in orthotopic canine model, Cancer Res. 69 (4) (2009) 1659–1667.
[155] M.P. Melancon, W. Lu, Z. Yang, R. Zhang, Z. Cheng, A.M. Elliot, J. Stafford, T. Olson, J.Z. Zhang, C. Li, In vitro and in vivo targeting of hollow gold nanoshells directed at epidermal growth factor receptor for photothermal ablation therapy, Mol. Cancer Ther. 7 (6) (2008) 1730–1739.
[156] W. Lu, C. Xiong, G. Zhang, Q. Huang, R. Zhang, J.Z. Zhang, C. Li, Targeted photothermal ablation of murine melanomas with melanocyte-stimulating hormone analog-conjugated hollow gold nanospheres, Clin. Cancer Res. 15 (3) (2009) 876–886.
[157] L.R. Hirsch, R.J. Stafford, J.A. Bankson, S.R. Sershen, B. Rivera, R.E. Price, J.D. Hazle, N.J. Halas, J.L. West, Nanoshell-mediated near-infrared thermal therapy of tumors under magnetic resonance guidance, Proc. Natl. Acad. Sci. USA 100 (23) (2003) 13549–13554.
[158] J.M. Stern, J. Stanfield, W. Kabbani, J.-T. Hsieh, J.A. Cadeddu, Selective prostate cancer thermal ablation with laser activated gold nanoshells, J. Urol. 179 (2) (2008) 748–753.
[159] G.P. Goodrich, L. Bao, K. Gill-Sharp, K.L. Sang, J. Wang, J.D. Payne, Photothermal therapy in a murine colon cancer model using near-infrared absorbing gold nanorods, J. Biomed. Opt. 15 (1) (2010).
[160] J. Chen, C. Glaus, R. Laforest, Q. Zhang, M. Yang, M. Gidding, M.J. Welch, Y. Xia, Gold nanocages as photothermal transducers for cancer treatment, Small 6 (7) (2010) 811–817.
[161] H.K. Moon, S.H. Lee, H.C. Choi, C. Nanotubes, In vivo near-infrared mediated tumor destruction by photothermal effect of carbon nanotubes, ACS Nano 3 (11) (2009) 3707–3713.
[162] C. Loo, A. Lowery, N. Halas, J. West, R. Drezek, Immunotargeted nanoshells for integrated cancer imaging and therapy, Nano Lett. 5 (4) (2005) 709–711.
[163] Y. Wang, Y. Liu, H. Luehmann, X. Xia, D. Wan, C. Cutler, Y. Xia, Radioluminescent gold nanocages with controlled radioactivity for real-time in vivo imaging, Nano Lett. 13 (2) (2013) 581–585.
[164] E.C. Cho, Y. Zhang, X. Cai, C.M. Moran, L. V Wang, Y. Xia, Quantitative analysis of the fate of gold nanocages in vitro and in vivo after uptake by U87-MG tumor cells, Angew. Chem. Int. Ed. Engl. 52 (4) (2013) 1152–1155.
[165] K. Maier-Hauff, R. Rothe, R. Scholz, U. Gneveckow, P. Wust, B. Thiesen, A. Feussner, A. von Deimling, N. Waldoefner, R. Felix, A. Jordan, Intracranial thermotherapy using magnetic nanoparticles combined with external beam radiotherapy: results of a feasibility study on patients with glioblastoma multiforme, J. Neurooncol. 81 (1) (2007) 53–60.
[166] M. Johannsen, U. Gneveckow, L. Eckelt, A. Feussner, N. WaldÖFner, R. Scholz, S. Deger, P. Wust, S.a. Loening, a. Jordan, Clinical hyperthermia of prostate cancer using magnetic nanoparticles: presentation of a new interstitial technique, Int. J. Hyperthermia 21 (7) (2005) 637–647.
[167] G.A. Sotiriou, A.M. Hirt, P.-Y. Lozach, A. Teleki, F. Krumeich, S.E. Pratsinis, Hybrid, silica-coated, janus-like plasmonic-magnetic nanoparticles, Chem. Mater. 23 (7) (2011) 1985–1992.
[168] X. Ji, R. Shao, A.M. Elliott, R.J. Stafford, E. Esparza-Coss, G. Liang, Z.P. Luo, K. Park, J.T. Markert, C. Li, Bifunctional gold nanoshells with a superparamagnetic iron oxide-silica core suitable for both MR imaging and photothermal therapy, J. Phys. Chem. C 111 (17) (2007) 6245–6251.
[169] W. Lu, A.K. Singh, S.A. Khan, D. Senapati, H. Yu, P.C. Ray, Gold nano-popcorn-based targeted diagnosis, nanotherapy treatment, and in situ monitoring of photothermal therapy response of prostate cancer cells using surface-enhanced Raman spectroscopy, J. Am. Chem. Soc. 132 (51) (2010) 18103–18114.
[170] R.M. Blaese, K.W. Culver, A.D. Miller, C.S. Carter, T. Fleisher, M. Clerici, G. Shearer, L. Chang, Y. Chiang, P. Tolstoshev, J.J. Greenblatt, S.A. Rosenberg, H. Klein, M. Berger, C.A. Mullen, W.J. Ramsey, L. Muul, R.A. Morgan, W.F. Anderson, T lymphocyte-directed gene therapy for ADA- SCID: initial trial results after 4 years, Science 270 (5235) (1995) 475–480 (New York, NY).
[171] S. Li, L. Huang, Nonviral gene therapy: promises and challenges, Gene Ther. 7 (1) (2000) 31–34.
[172] P.L. Felgner, T.R. Gadek, M. Holm, R. Roman, H.W. Chan, M. Wenz, J.P. Northrop, G.M. Ringold, M. Danielsen, Lipofection: a highly efficient, lipid-mediated DNA-transfection procedure, Proc. Nat. Acad. Sci. USA 84 (21) (1987) 7413–7417.
[173] X. Duan, P. Wang, K. Men, X. Gao, M. Huang, M. Gou, L. Chen, Z. Qian, Y. Wei, Treating colon cancer with a suicide gene delivered by self-assembled cationic MPEG-PCL micelles, Nanoscale 4 (7) (2012) 2400–2407.